Supporting Information

Evolving a Unique Red-Emitting Fluorophore with an Optically Tunable Hydroxy Group for Imaging Nitroreductase in Cells, in Tissues, and in Vivo

Rong Peng,[†+] Jie Yuan,[†+] Dan Cheng,[†+] Tianbing Ren,[†] Fangping Jin,[†] Ronghua Yang,[‡] Lin Yuan,[†*] and Xiaobing Zhang[†]

[†]State Key Laboratory of Chemo/Biosensing and Chemometrics, College of Chemistry and Chemical Engineering, Hunan University, Changsha 410082 (PR China)

[+]Equal contribution; [*]Email: lyuan@hnu.edu.cn.

[‡]School of Chemistry and Biological Engineering, Changsha University of Science and Technology, Changsha, China (PR China)

Table of contents

1. Materials and General Experimental Methods

Unless otherwise stated, all reagents were purchased from commercial suppliers and used without further purification. Solvents used were purified by standard methods prior to use. Twice-distilled water was used throughout all experiments. NTR, NADH and dicoumarin (DC) were purchased from Sigma. The NTR powder and NADH was dissolved into pure water to form aqueous solution and was divided into several parts for daily experiments. To keep the enzyme activity, all these solutions were stored at -80 °C before use according to a reported procedure.[1] Dicoumarin was dissolved in DMSO. Mass spectra were performed using an LCQ advantage ion trap mass spectrometer from Thermo Finnigan. NMR spectra were recorded on a Bruker-400 spectrometer, using TMS as an internal standard. High-resolution electronspray (ESI-HRMS) mass spectra were obtained from The Thermo Fisher Scientific LTQ FT Ultra (Shanghai Institute of Organic Chemistry Chinese Academic of Sciences). Photoluminescent spectra were recorded at room temperature with a HITACHI F4600 fluorescence spectrophotometer (1 cm standard quartz cell). The pH measurements were carried out on a Mettler-Toledo Delta 320 pH meter; the fluorescence images were acquired with a two photon confocal laser scanning microscope (Nikon, Japan); The *in vivo* (living mice) imaging was carried out using an IVIS Lumina XR (IS1241N6071) *in vivo* imaging system; TLC analysis was performed on silica gel plates and column chromatography was conducted over silica gel (mesh 100–200), both of which were obtained from the Qingdao Ocean Chemicals.

2. Determination of fluorescence quantum yield.

Fluorescence quantum yield for **ACF4**, **LDOH-1-4**, and **Ctrl 1-2** was determined by using cresyl violet ($\Phi_f = 0.54$ in methanol) as a fluorescence standard.[2] The quantum yield was calculated using the following equation:

$$\Phi_{F(X)} = \Phi_{F(S)}(A_S F_X / A_X F_S)\,(n_X / n_S)^2 \qquad (1)$$

Where Φ_F is the fluorescence quantum yield, A is absorbance, F is relative integrated fluorescence intensity, and n is the refractive index of the solvents used. Subscripts S and X refer to the standard and to the unknown, respectively.

3. DFT calculations.

To describe the excited state of fluorophores **LDOH-1** and **LDOH-2**, time-dependent density functional theory (TD-DFT) calculations were performed. The calculations were carried out using the Gaussian 09 program package. All the geometries of fluorophores were optimized at B3LYP/6-311+ G (d, p) level using a CPCM solvation model with water as the solvent. The molecular orbital (MO) plots and MO energy levels were computed at the same level of theory.

4. Detection Limit Calculation.

The detection limit was calculated based on the fluorescence titration. The detection limit is calculated using the following equation:

$$\text{Detection limit} = 3\sigma/k \quad (2)$$

where σ is the standard deviation of blank measurements, k is the slope between the emission versus sample concentration.

5. Measurement of Two-Photon Absorption Cross Section.

The two-photon absorption action cross-section of **LDOH-4** was determined using Rhodamine B in methanol as the reference molecules.[3] The two-photon absorption cross section was determined by equation:

$$\sigma = \sigma_r(F_t n_t^2 \Phi_r C_r)/(F_r n_r^2 \Phi_t C_s) \quad (3)$$

where the subscripts t and r stand for the sample and reference molecules, F is the average fluorescence intensity, n is the refractive index of the solvent, C is the concentration, Φ is the quantum yield, and σ_r is the two-photon cross-section of the reference molecule.

6. Synthesis and Characterization

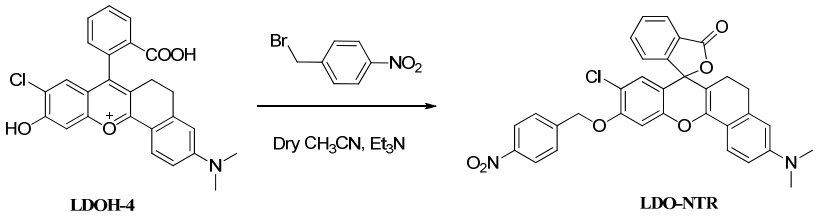

Scheme S1. Synthetic route of **LDO-NTR**.

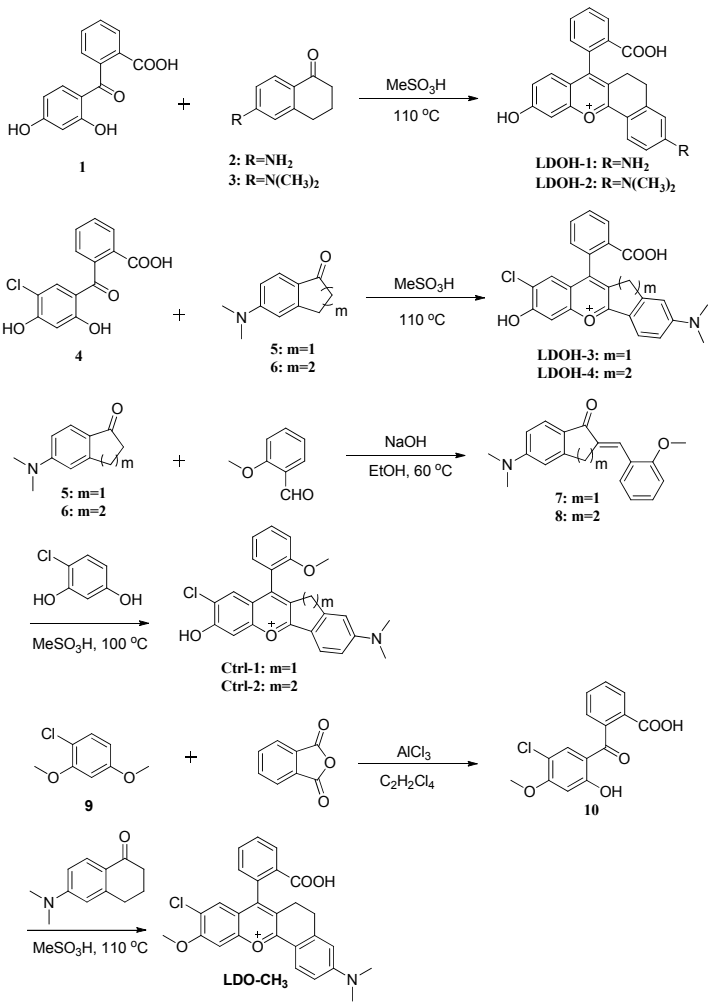

Scheme S2. Synthetic route of **LDOH-1-4, Ctrl-1-2** and **LDO-CH$_3$**.

Synthesis of LDOH-1. Compound **1** was prepared by reported method.[4] The synthetic method of **LDOH-1** was similar to **LDOH-4**. **LDOH-1**: Yield: 26% (red solid). ^{1}H NMR (400 MHz, CD_3OD) δ 8.04 (s, 1H), 7.90 (d, J = 8.6 Hz, 1H), 7.57 (s, 2H), 7.16 (s, 1H), 7.00 (d, J = 9.1 Hz, 1H), 6.73 – 6.62 (m, 3H), 6.52 (s, 1H), 2.85 (m, 1H), 2.80 – 2.72 (m, 1H), 2.71 – 2.58 (m, 1H), 2.55 – 2.43 (m, 1H). ^{13}C NMR (100 MHz, CD_3OD) δ 180.3, 172.6, 162.1, 161.6, 159.0, 154.9, 144.4, 139.0, 133.8, 129.5, 129.4, 129.3, 128.7, 128.1, 127.7, 125.2, 116.4, 115.1, 114.9, 113.1, 112.2, 102.5, 27.1, 23.6. MS (ESI): calcd for $C_{24}H_{18}NO_4^+$ [M^+] 384.1, found 384.3.

Synthesis of LDOH-2. The synthetic method of **LDOH-2** was similar to **LDOH-1**. **LDOH-2**: Yield: 32% (red solid). ^{1}H NMR (400 MHz, DMSO-d_6) δ 8.11 (d, J = 7.7 Hz, 1H), 7.99 (d, J = 7.9 Hz, 1H), 7.83 (t, J = 7.5 Hz, 1H), 7.73 (t, J = 7.5 Hz, 1H), 7.38 (d, J = 7.6 Hz, 1H), 7.20 (s, 1H), 6.88 (t, J = 11.0 Hz, 2H), 6.78 (d, J = 8.6 Hz, 1H), 6.71 (s, 1H), 3.13 (s, 6H), 2.84 – 2.77 (m, 2H), 2.25 (s, 2H). ^{13}C NMR (100 MHz, DMSO-d_6) δ 169.6, 157.6, 154.12, 151.7, 139.3, 136.5, 133.2, 131.0, 129.4, 128.9, 128.1, 127.4, 126.8, 125.3, 124.3, 115.6, 115.4, 110.9, 110.5, 110.1, 102.4, 27.7, 21.8, 18.6. MS (ESI): calcd for $C_{26}H_{22}NO_4^+$ [M^+] 412.2, found 412.3.

Synthesis of LDOH-3. Compound **4** was prepared by reported method.[4] The synthetic method of **LDOH-3** was similar to **LDOH-1**. **LDOH-3**: Yield: 42% (purple solid)**.** ^{1}H NMR (400 MHz, CD_3OD) δ 8.50 (d, J = 6.5 Hz, 1H), 8.17 (d, J = 8.8 Hz, 1H), 8.03 – 7.88 (m, 2H), 7.55 (d, J = 4.8 Hz, 1H), 7.42 (d, J = 5.5 Hz, 2H), 7.23 (d, J = 8.1 Hz, 1H), 7.08 (s, 1H), 3.86 (s, 2H), 3.54 (s, 6H).

^{13}C NMR (100 MHz, CD_3OD+$CDCl_3$) δ 157.3, 155.2, 155.2, 154.1, 153.8, 134.2, 132.9, 132.6, 132.1, 130.8, 129.6, 127.9, 126.7, 125.7, 120.3, 116.0, 115.4, 108.2, 108.2, 105.0, 41.0, 32.8. MS (ESI): calcd for $C_{25}H_{19}ClNO_4^+$ [M^+] 432.1, found 432.3.

Synthesis of compound 5. Compound **5** was prepared by reported method.[5] ^{1}H NMR (400 MHz, CD_3OD) δ 7.52 (d, *J* = 8.8 Hz, 1H), 6.77 – 6.62 (m, 2H), 3.12 – 2.92 (m, 8H), 2.63 – 2.53 (m, 2H).

Synthesis of compound 6. Compound **6** was prepared by the followed method.[5] ^{1}H NMR (400 MHz, CD_3OD) δ 7.80 (d, *J* = 8.9 Hz, 1H), 6.72 – 6.38 (m, 2H), 3.04 (s, 6H), 2.86 (t, *J* = 5.8 Hz, 2H), 2.50 (t, *J* = 6.2 Hz, 2H), 2.16 – 1.91 (m, 2H).

Synthesis of compound 7. Compound **5** (402.5 mg, 2.3 mmol), 2-methoxybenzaldehyde (408 mg, 3.0 mmol) and NaOH (3 mL) were dissolved with EtOH in 50 mL flask, stirring at 60 ^{o}C for 8 h. The reaction solution was evaporated, and the residue was chromatographed on silica gel with CH_2Cl_2 : EtOH (30:1) as the eluent to give compound **7** (400 mg, 59%) as a yellow powder. ^{1}H NMR (400 MHz, $CDCl_3$) δ 8.28 (s, 1H), 8.08 (d, *J* = 6.9 Hz, 1H), 7.94 (s, 1H), 7.63 (s, 1H), 7.37 – 7.17 (m, 1H), 7.05 – 6.87 (m, 1H), 4.18 (d, *J* = 9.5 Hz, 1H), 3.39 (s, 1H).

Synthesis of compound 8. The synthetic method of compound **8** was similar to compound **7**. compound **8:** Yield: 51% (yellow powder). ^{1}H NMR (400 MHz, $CDCl_3$) δ 8.07 (d, *J* = 7.3 Hz, 1H), 7.91 (s, 1H), 7.29 (d, *J* = 5.6 Hz, 3H), 7.05 – 6.86 (m, 2H), 6.64 (d, *J* = 7.0 Hz, 1H), 6.38 (s, 1H), 3.85 (s, 3H), 3.03 (d, *J* = 26.8 Hz, 10H), 2.87 (s, 2H).

Synthesis of Ctrl-1. The synthetic method of **Ctrl-1** was similar to **LDOH-1**. **Ctrl-1**: Yield: 46% (drak-purple solid)**.** ^{1}H NMR (400 MHz, CD_3OD) δ 8.32 (d, *J* = 8.8 Hz, 1H), 8.10 (t, *J* = 7.2 Hz, 1H), 7.96 (s, 1H), 7.77 (d, *J* = 6.1 Hz, 1H), 7.69 (d, *J* = 6.7 Hz, 2H), 7.46 (s, 1H), 7.37 (d, *J* = 8.7 Hz, 1H), 7.29 (s, 1H), 4.33 (s, 3H), 4.15 (q, *J* = 21.5 Hz, 2H), 3.69 (s, 6H). ^{13}C NMR (100 MHz, CD_3OD+$CDCl_3$) δ 170.6, 167.6, 156.3, 155.5, 154.2, 150.4, 148.9, 131.1, 129.2, 128.5, 126.2, 123.8, 123.7, 120.6, 120.1, 119.5, 112.7, 112.5, 110.9, 106.5, 103.9, 54.7, 39.5, 31.9. MS (ESI): calcd for $C_{25}H_{21}ClNO_3^+$ [M^+] 418.1, found 418.2.

Synthesis of Ctrl-2. The synthetic method of **Ctrl-2** was similar to **LDOH-1**. **Ctrl-2**: Yield: 48% (dark purple solid)**.** ^{1}H NMR (400 MHz, CD_3OD) δ 8.08 (d, *J* = 9.1 Hz, 1H), 7.73 (m, 1H), 7.36 – 7.29 (m, 4H), 6.98 (s, 1H), 6.84 (dd, *J* = 9.1, 2.0 Hz, 1H), 6.68 (s, 1H), 3.97 (s, 3H), 3.29 (s, 6H), 3.03 (t, *J* = 7.5 Hz, 2H), 2.83 (m, 1H), 2.72 (m, 1H). ^{13}C NMR (100 MHz, CD_3OD+$CDCl_3$) δ 163.05, 157.44, 156.86, 155.27, 154.49, 145.00, 133.83, 132.21, 130.34, 130.19, 128.66, 127.62, 122.32, 121.55, 118.41, 115.80, 114.70, 112.14, 111.05, 108.37, 104.22, 55.99, 40.37, 30.16, 28.49. MS (ESI): calcd for $C_{26}H_{23}ClNO_3^+$ [M^+] 432.1, found 432.2.

Synthesis of compound 10. Compound **9** was prepared by reported method.[6] $AlCl_3$ (1.2 g, 9.1 mmol) and phthalic anhydride (520 mg, 3.5 mmol) were dissolved with tetrachloroethane (10 mL) in 35 mL pressure tube, stirring at 0 ^{o}C for 1 h. Then compound **9** (516 mg, 3 mmol) was added to the above solution, stirring at 100 ^{o}C for about 10 h. The reaction solution was poured into the mixture of ice water and stirred continuously, a yellow solid product was obtained by filtration. The product was directly used for the next step.

Synthesis of LDO-CH_3. The synthetic method of **LDO-CH_3** was similar to **LDOH-1**. **LDO-CH_3**: Yield: 43% (drak-purple solid)**.** ^{1}H NMR (400 MHz, CD_3OD) δ 8.19 – 8.14 (m, 1H), 8.11 (d, *J* = 9.2 Hz, 1H), 7.67 (dd, *J* = 5.3, 3.6 Hz, 2H), 7.43 (s, 1H), 7.22 – 7.16 (m, 1H), 7.12 (s, 1H), 6.83 (dd, *J* = 9.2, 2.5 Hz, 1H), 6.65 (d, *J* = 2.1 Hz, 1H), 4.08 (s, 3H), 3.24 (s, 6H), 3.07 – 2.97 (m, 1H), 2.96 – 2.86 (m, 1H), 2.79 – 2.67 (m, 1H), 2.64 – 2.53 (m, 1H). ^{13}C NMR (100 MHz, CD_3OD+$CDCl_3$) δ 163.3, 159.2, 155.8, 153.0, 147.5, 146.1, 136.9, 136.1, 130.9, 130.8, 129.5,

129.4, 129.4, 127.8, 126.8, 122.5, 119.3, 117.2, 114.0, 112.6, 110.7, 100.4, 56.7, 39.7, 29.4, 27.4. MS (ESI): calcd for $C_{27}H_{23}ClNO_4^+$ [M^+] 460.1, found 460.2.

7. Spectrometric Studies

Measurement of photophysical properties. For photophysical characterization, all dyes (**LDOH-1-4**, **Ctrl-1-2** and **LDO-CH$_3$**) and the probe **LDO-NTR** were dissolved in DMSO to make the stock solutions (500 μM). The **LDOH-1-4**, **Ctrl-1-2** and **LDO-CH$_3$** were diluted to 5 μM as the testing solutions with PBS buffer solution (25 mM, 20% DMSO). The probe **LDO-NTR** was diluted to 5 μM as the testing solutions with PBS buffer solution (25 mM, 1% DMSO, pH=7.4). Absorption and fluorescence spectroscopic studies were performed on a Labtech UV Power PC spectrometer; a Hitachi F-4600 fluorescence spectrophotometer. Sources for different ROS/RNS are described as follows. Specifically, H_2O_2 solution was purchased from Sigma-Aldrich and added into the probe solution directly. Superoxide ($O_2^{\bullet-}$) was generated from KO_2 was dissolved in DMSO. The source of NaOCl was commercial bleach.

8. Fluorescence Microscopic Studies

Cell culture. HepG2 cells were cultured in high glucose Dulbecco's Modified Eagle Medium (DMEM, Hyclone) supplemented with 10% fetal bovine serum (FBS, BI), and 1% antibiotics (100 U/mL penicillin and 100 μg/mL streptomycin, Hyclone) at 37 °C and 5% CO_2. Cells werecarefully harvested and split when they reached 80% confluence to maintain exponential growth.

Cytotoxicity Study of LDO-NTR for HepG2 Cells. The cytotoxic effects of **LDO-NTR** was determined by MTT [3-(4,5-dimethyl-2-thiazolyl)-2,5-diphenyl-2H-tetrazolium bromide] assay. HepG2 cells (1×10^4 cells/well) were placed in a flat-bottom 96-well plate in 100 μL of culture medium and incubated in 5% CO_2 at 37 °C for 24 h. The cells were treated with different concentrations (0−10 μM) of **LDO-NTR**. After 24 h of incubation, MTT solution (5.0 mg/mL) was added into each well (0.5 mg/mL). Residual MTT solution was removed after 4 h, and then dimethyl sulfoxide (DMSO, 100 μL) was added to each well to dissolve the formazan crystals. After the plates were shaken for 10 min, the absorbance values of the wells were recorded by use of a microplate reader at 490 nm. The cytotoxic effects (VR) of **LDO-NTR** were assessed by the following equation: $VR = A/A_0 \times 100$, where A and A_0 represent absorbance of the experimental group and control group, respectively. The assays were performed in six sets for each concentration.

Fluorescence microscopy imaging. To avoid the artifacts that occur during fixation procedures, all the experiments were conducted in live cells. HepG2 cells were first cultured under normoxic (20% O_2) and different hypoxic conditions (10% and 1% O_2) for 5 hours. Then HepG2 cells were incubated with **LDO-NTR** (5 μM) for 30 min at 37 °C and washed with PBS three times before imaging. One-photon and TP excited fluorescence imaging of HepG2 cells was performed by a confocal laser scanning microscope (CLSM, C1-Si, Nikon, Japan) with an excitation filter of 561 nm and the collection wavelength range is from 570-620 nm, respectively, and TP images were performed with a mode-locked titanium-sapphire laser source set at a wavelength of 820 nm and the collection wavelength range is from 570-620 nm, respectively.

Fluorescence imaging in hypoxic tumor mice model. 4T1 breast cancer mice model were used fluorescence imaging. 4T1 breast cancer model preparation procedures were in accordance with the guidelines of the institutional animal use and care regulations (No. SYXK (Xiang) 2008-0001).

9. Supplemental Figures

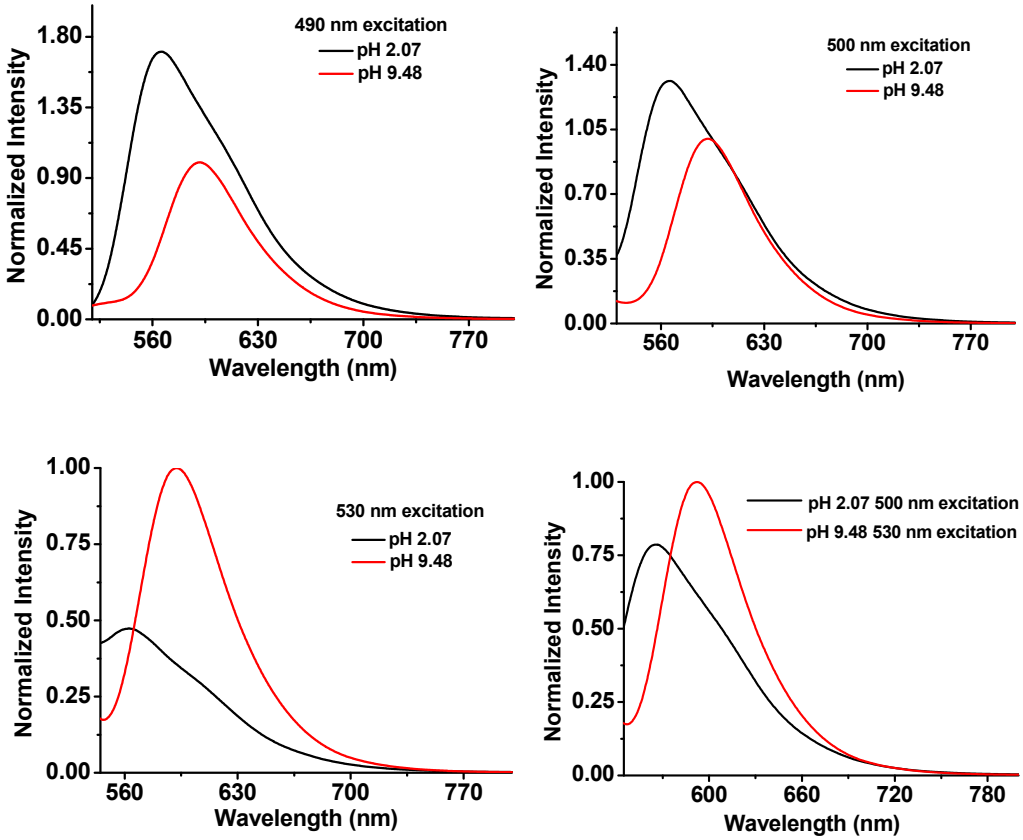

Figure S1. Normalized fluorescence emission of **ACF4** (5 μM) with different pH (2.07 and 9.48) in PBS buffer solution (25 mM, DMSO : PBS=2 : 8) at different excitation wavelength.

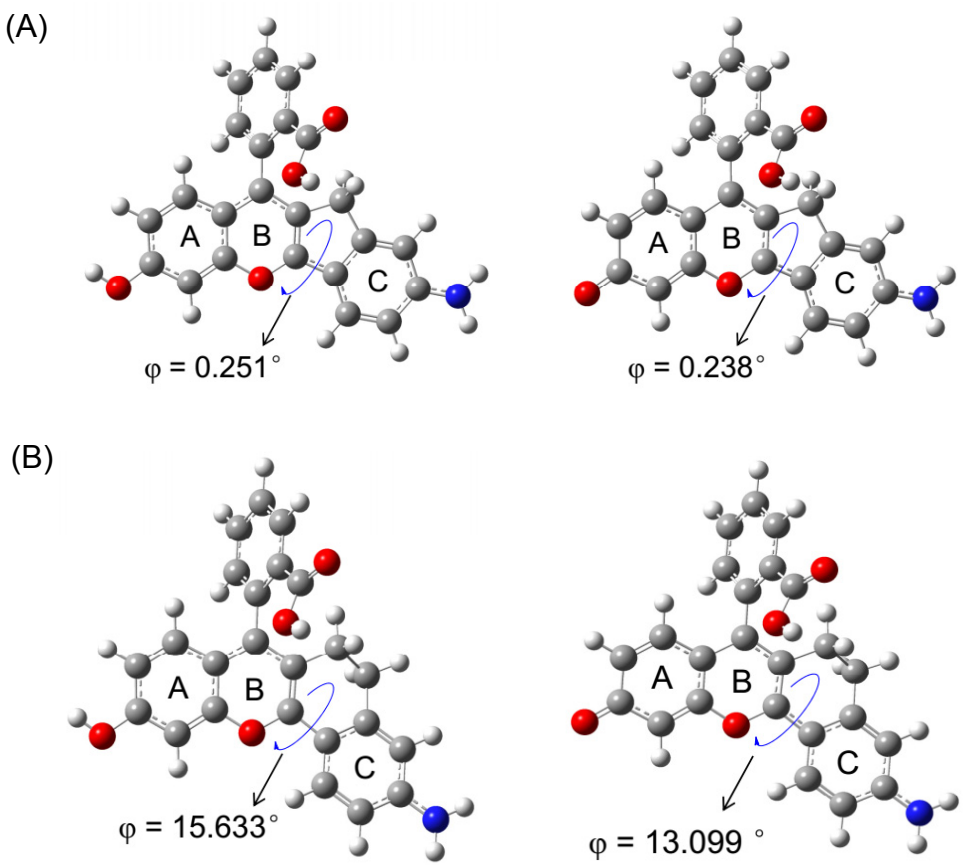

Figure S2. (A) The optimized molecular structure of **ACF4** at the phenol state and phenolate state. The molecular planarity was plotted with different twist angles (φ) at the bridging bond of five-membered ring in water. (B) The optimized molecular structure of **LDOH-1** at the phenol state and phenolate state. The molecular planarity was plotted with different twist angles (φ) at the bridging bond of six-membered ring in water. A, B and C represented three rings of the chemical modification.

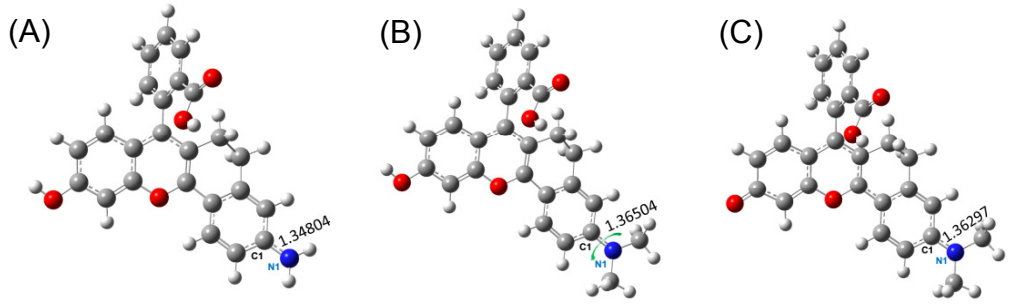

Figure S3. The optimized molecular structure of amino **LDOH-1** and **LDOH-2** and bond distances of C1-N1 bond at the phenol state for **LDOH-1** (A) and **LDOH-2** (B) and phenolate state for **LDOH-2** (C), respectively. The calculation was performed at B3LYP/6-311 + G (d, p) level using a CPCM solvation model with water as the solvent at excited state.

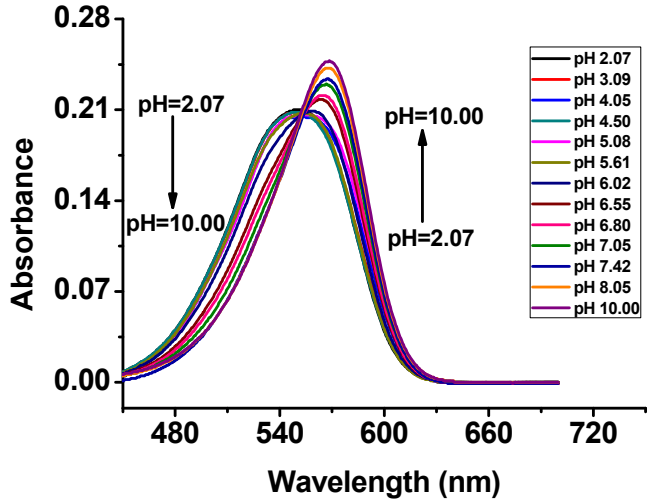

Figure S4. Absorption spectra of **LDOH-2** (5 μM) in PBS buffer solution (25 mM, DMSO : PBS=2 : 8) with pH changing from 2.07 to 10.00.

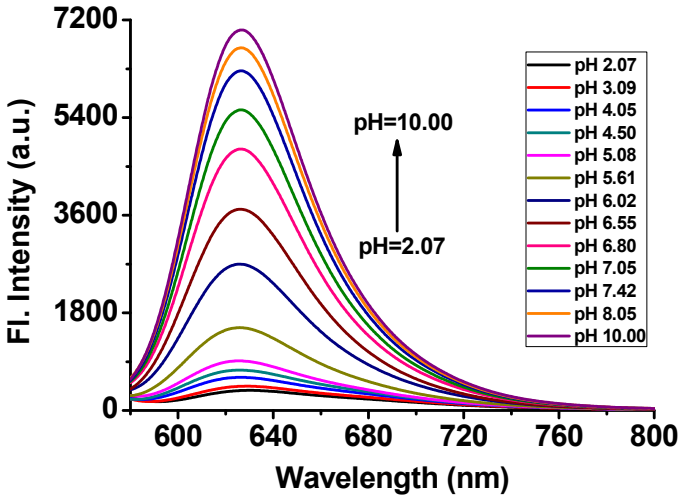

Figure S5. Fluorescence emission spectra of **LDOH-2** (5 μM) in PBS buffer solution (25 mM, DMSO : PBS=2 : 8) with pH changing from 2.07 to 10.00, λ_{ex} = 561 nm.

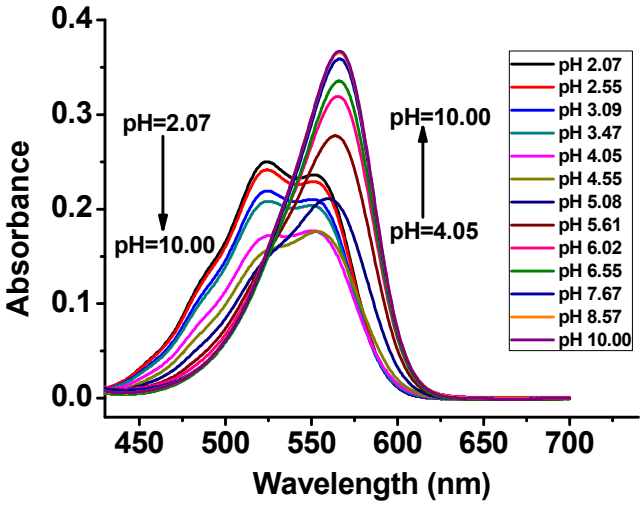

Figure S6. Absorption spectra of **LDOH-3** (5 μM) in PBS buffer solution (25 mM, DMSO : PBS=2 : 8) with pH changing from 2.07 to 10.00.

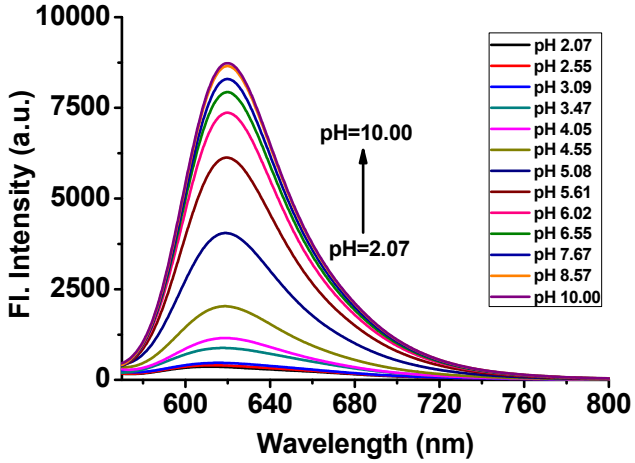

Figure S7. Fluorescence emission spectra of **LDOH-3** (5 μM) in PBS buffer solution (25 mM, DMSO : PBS=2 : 8) with pH changing from 2.07 to 10.00, λ_{ex} = 550 nm.

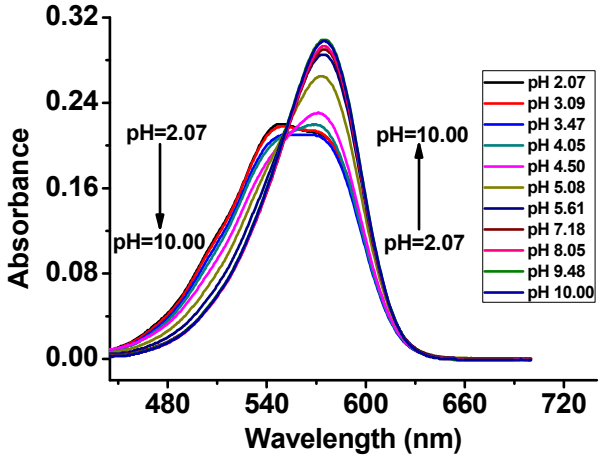

Figure S8. Absorption spectra of **LDOH-4** (5 μM) in PBS buffer solution (25 mM, DMSO : PBS=2 : 8) with pH changing from 2.07 to 10.00.

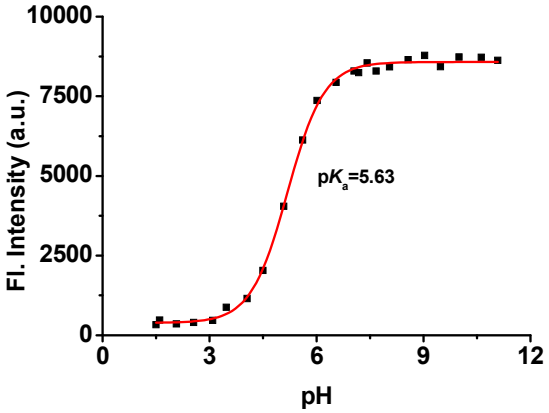

Figure S9. pK_a of **LDOH-3** (5 μM) in PBS buffer solution (25 mM, DMSO : PBS=2 : 8) with pH changing from 1.50 to 11.08, λ_{ex} = 550 nm.

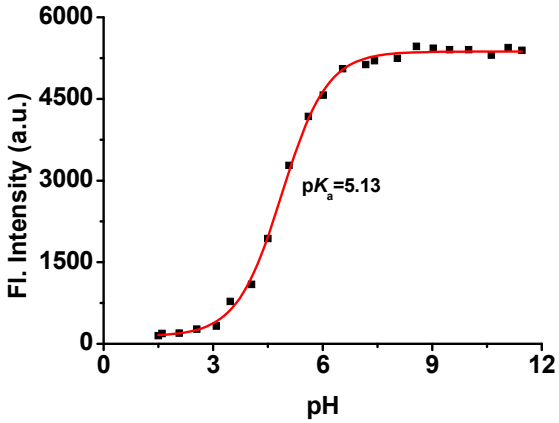

Figure S10. pK_a of **LDOH-4** (5 μM) in PBS buffer solution (25 mM, DMSO : PBS=2 : 8) with pH changing from 1.50 to 11.46, λ_{ex} = 561 nm.

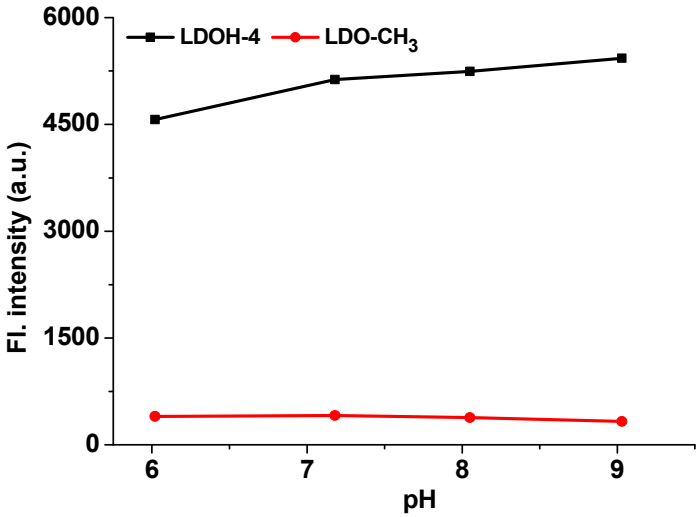

Figure S11. Fluorescence intensity of **LDOH-4** and **LDO-CH$_3$** (5 μM) in PBS buffer solution at different pH (25 mM, DMSO : PBS=2 : 8).

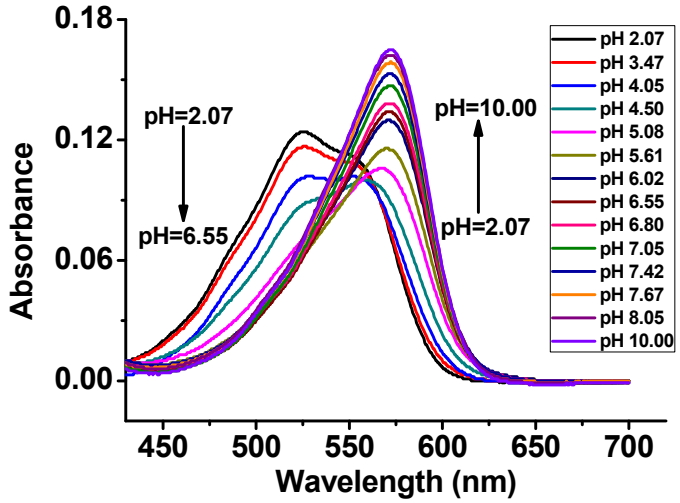

Figure S12. Absorption spectra of **Ctrl-1** (5 μM) in PBS buffer solution (25 mM, DMSO : PBS=2 : 8) with pH changing from 2.07 to 10.00.

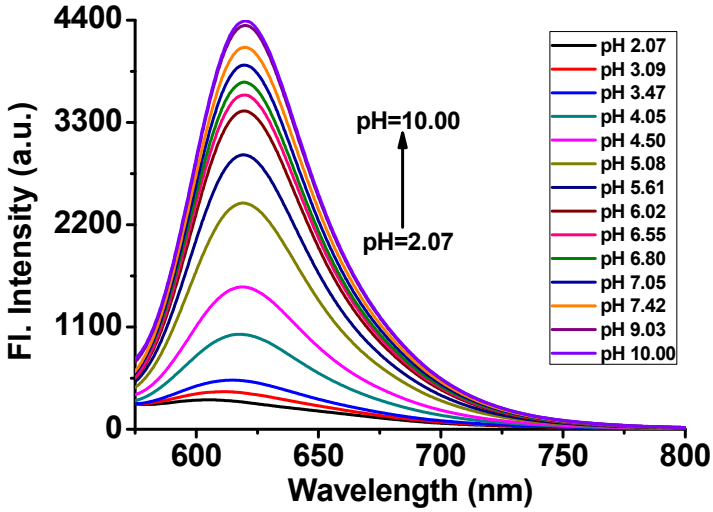

Figure S13. Fluorescence emission spectra of **Ctrl-1** (5 μM) in PBS buffer solution (25 mM, DMSO : PBS=2 : 8) with pH changing from 2.07 to 10.00, λ_{ex} = 550 nm.

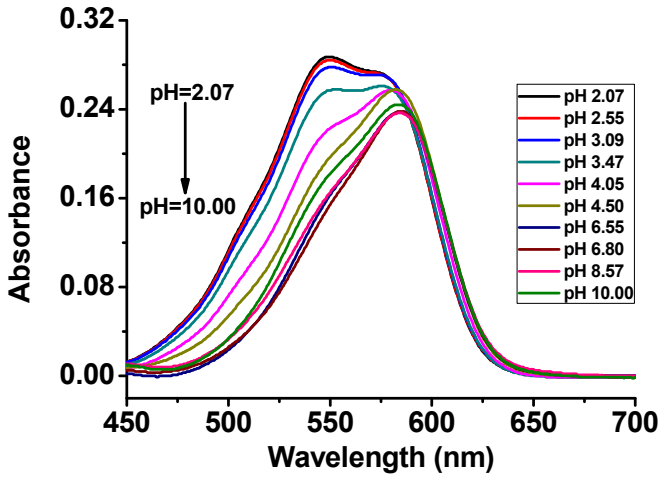

Figure S14. Absorption spectra of **Ctrl-2** (5 μM) in PBS buffer solution (25 mM, DMSO : PBS=2 : 8) with pH changing from 2.07 to 10.00.

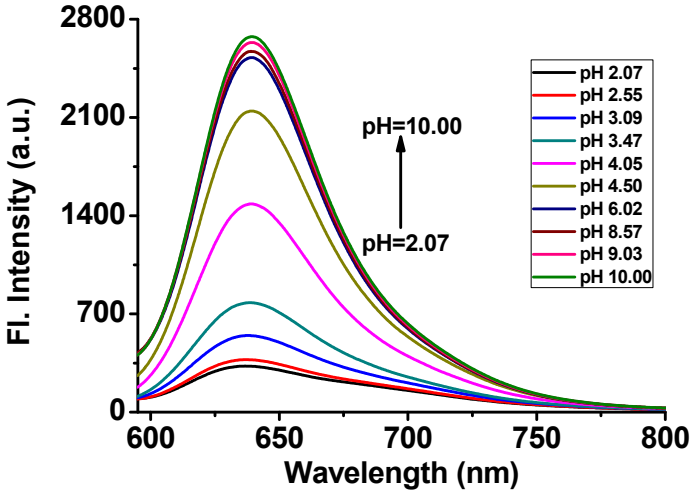

Figure S15. Fluorescence emission spectra of **Ctrl-2** (5 μM) in PBS buffer solution (25 mM, DMSO : PBS=2 : 8) with pH changing from 2.07 to 10.00, λ_{ex} = 561 nm.

Table S1. Photo-physical properties of **ACF4**, **LDOH-1-4** and **Ctrl-1-2**.

Compound	λ_{ab} (nm)[a]	λ_{em} (nm)[a]	Stokes shift (nm)[a]	ε ($M^{-1}cm^{-1}$)[b]	Φ[b]	pK_a	FEF[c]
ACF4	533	590	57	3.04×10^4	0.96	7.0	1.6
LDOH-1	542	601	59	1.56×10^4	0.72	6.0	3.1
LDOH-2	568	627	59	4.96×10^4	0.55	6.5	19.1
LDOH-3	566	620	54	7.40×10^4	0.70	5.6	23.7
LDOH-4	574	633	59	6.00×10^4	0.55	5.1	27.8
Ctrl-1	572	620	48	3.30×10^4	0.57	6.0	14.8
Ctrl-2	584	639	55	4.90×10^4	0.31	4.6	7.9

[a] Tested in PBS buffer solution (25 mM, pH 7.4, 20% DMSO). [b] Tested in PBS buffer solution (25 mM, pH 10.0, 20% DMSO). [c] Fluorescence enhancement factor (FEF) of dyes at pH 9.48 to 2.07 tested in PBS buffer solution (25 mM, 20% DMSO).

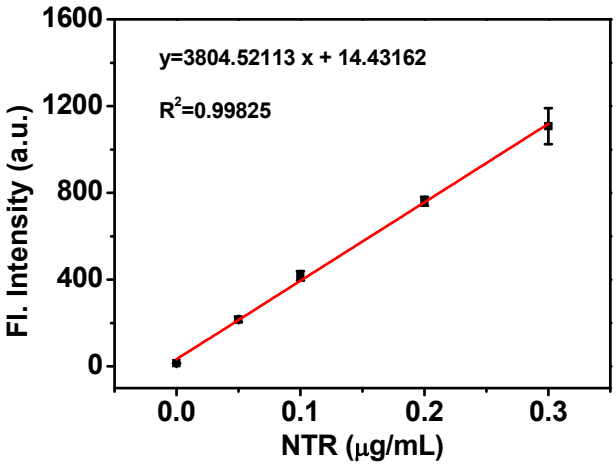

Figure S16. Linear correlation between the concentration of NTR and the fluorescence intensity of the reaction mixture ($\lambda_{ex}/\lambda_{em}$ = 561/624 nm), data shown as mean ± s.d. (n = 3).

Table S2. Properties of respresentative fluorescent probes for NTR

Probes	λ_{ex}/nm	λ_{em}/nm	LOD	Michaelis constant (K_m)	Response time	Bioimaging application
1[7]	398	494	20 ng/mL	48.07 μM	20 min	cell tissue
1[8]	470	520	9.6 ng/mL	36.29 μM	5 min	cell escherichia coli
Cy7-1[9]	730	782	1.14 ng/mL	190.3 μM	3 min	cell in vivo
FNTR[10]	410	560	23.67 ng/mL	~	10 min	cell tissue zebrafish
PBFBT-NP[11]	430	530	2.9 ng/mL	~	6 min	cell escherichia coli
PyCL-NO_2[12]	467	526	27 ng/mL	72.28 μM	60 min	cell
1[13]	550	604	2.2 ng/mL	~	10 min	cell
1[14]	345	475/ 550	0.77 ng/mL	~	20 min	cell
1[15]	515	550	51.5 ng/mL	~	60 min	cell c. elegans
1[16]	658	699	8.4 ng/mL	7.21 μM	30 min	bacteria cell
(1)[17]	~	537	24.5 ng/mL	~	24 min	cell tissue
FBN-1[18]	490	515	0.66 ng/mL	~	5 min	cell in vivo
Lyso-NTR[19]	425	543	2.2 ng/mL	45.6 μM	~	cell
CoNO_2-HY[20]	380	511	20 ng/mL	~	20 min	cell slices
NBP[21]	580	658	180 ng/mL	~	~	cell

1[22]	670	705	14 ng/mL	32.2 μM	15 min	cell zebrafish
CyNNO$_2$[23]	689	747/805	0.0058 ng/mL	~	20 min	cell
1[24]	605	720	~	18.28 μM	10 min	cell
(5)[25]	590	708	~	301.8 μM	20 min	response assays (in vitro)
1[26]	620	657	36.9 ng/mL	40.75 μM	~	bacterial pathogens
LDO-NTR (this work)	561	624	0.79 ng/mL	35.07 μM	15 min	cell tissues in vivo

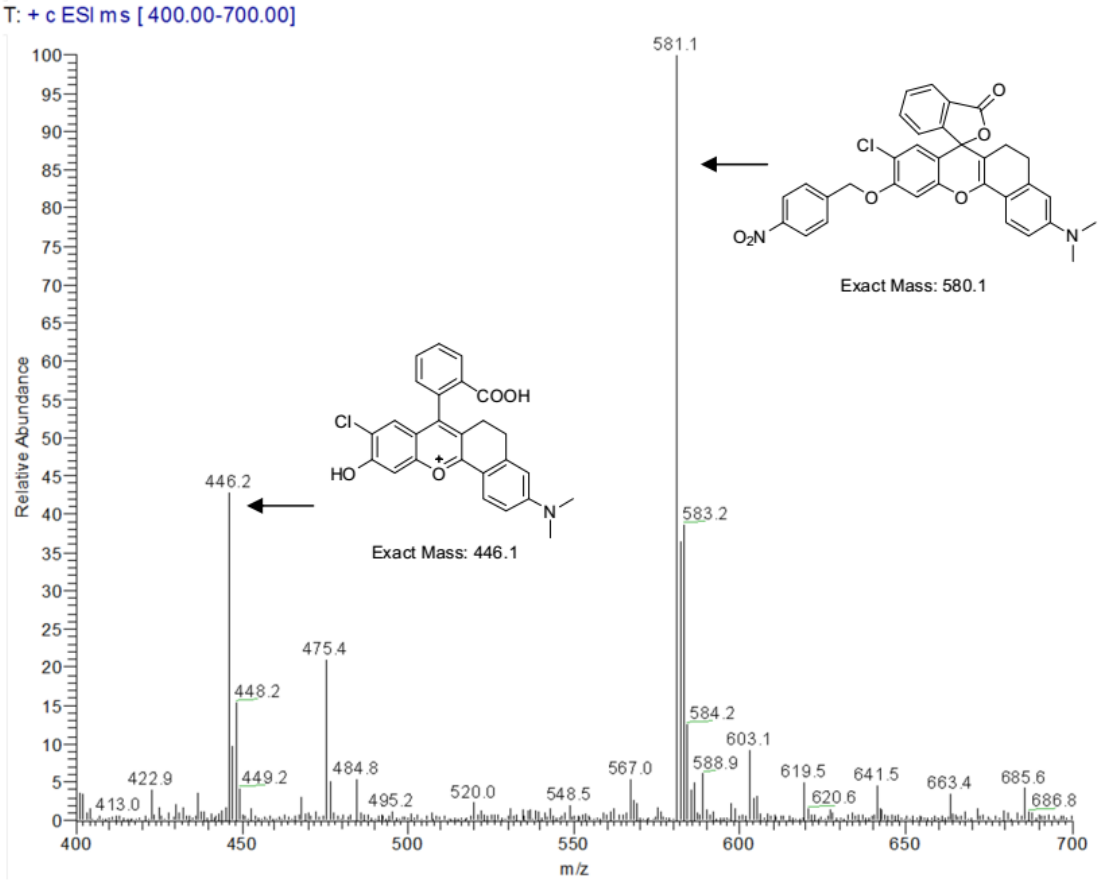

Figure S17. The ESI mass spectrum of **LDO-NTR** in the presence of NTR + NADH.

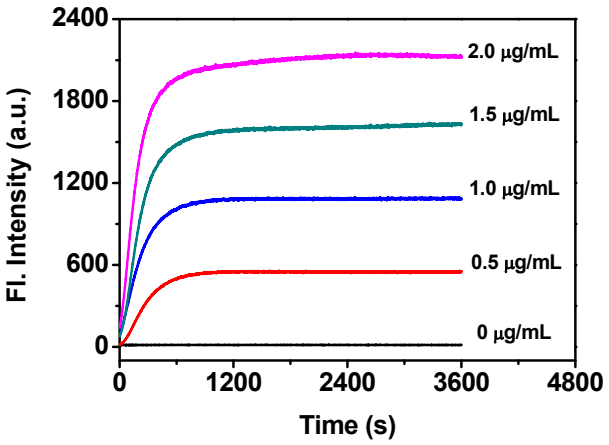

Figure S18. Time dependent fluorescence emission intensity of **LDO-NTR** (5 μM) after reaction with different concentrations of NTR (0, 0.5, 1.0, 1.5, 2.0 μg/mL) in the presence of 500 μM NADH. λ_{ex} = 561 nm, λ_{em} = 624 nm.

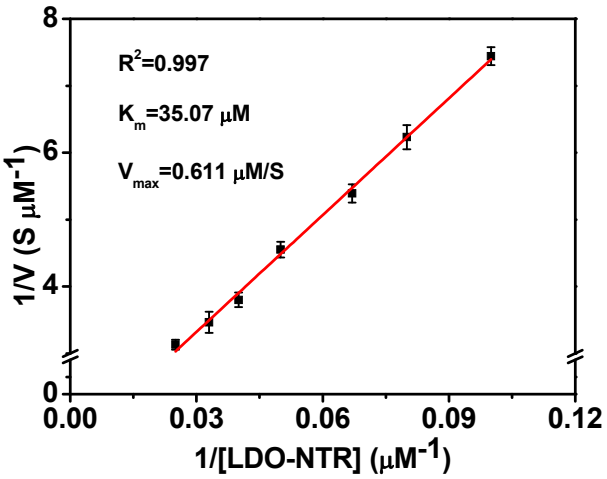

Figure S19. Lineweaver-Burk plot for the enzyme-catalyzed reaction. The Michaelis-Menten equation was described as: $V = V_{max}$[probe] / (K_m+[probe]), where V is the reaction rate, [probe] is the probe concentration (substrate), and K_m is the Michaelis constant. Conditions: 2 μg mL^{-1} nitroreductase, 500 μM NADH, 10-40 μM of **LDO-NTR** at 37 ^{o}C. Reaction at each probe concentration was repeated three times, and the error bars represent standard deviations.

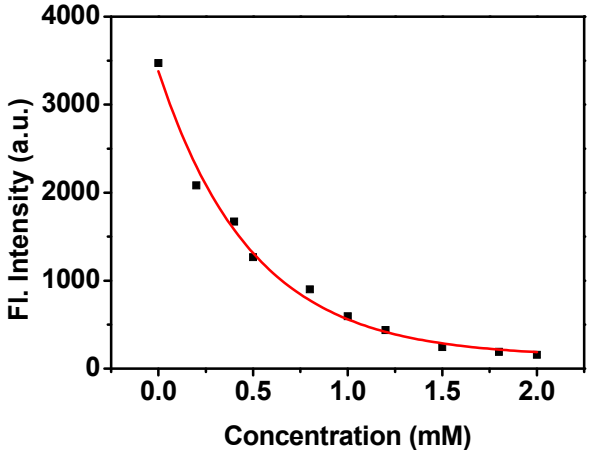

Figure S20. Effect of dicoumarin on the fluorescence intensity of **LDO-NTR** (5 μM) reacted with nitroreductase (0 and 2 μg/mL) + NADH (500 μM) + dicoumarin (0~2.0 mM) in PBS for 40 min at 37 ^{o}C .λ_{ex} = 561 nm. λ_{em} = 624 nm.

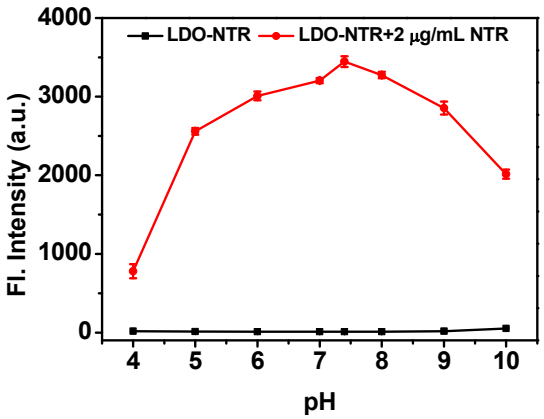

Figure S21. Effect of pH on the fluorescence intensity of **LDO-NTR** (5 μM) reacted with nitroreductase (2 μg/mL) + NADH (500 μM) in PBS (25 mM, 1% DMSO, pH=7.4) for 40 min at 37 ^{o}C. $\lambda_{ex}/\lambda_{em}$ = 561/624 nm.

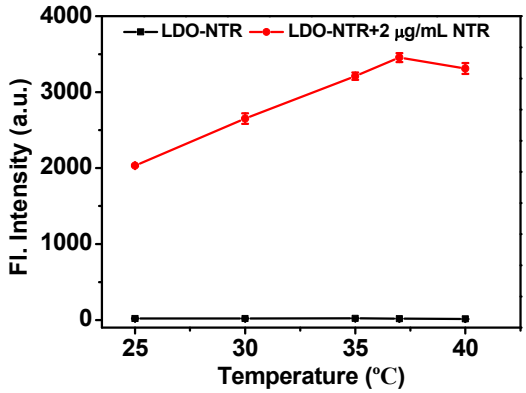

Figure S22. Fluorescence intensity of **LDO-NTR** (5 μM) reacted with nitroreductase (2 μg/mL) + NADH (500 μM) in PBS (25 mM, 1% DMSO, pH=7.4) for 40 min at different temperature (B). $\lambda_{ex}/\lambda_{em}$ = 561/624 nm.

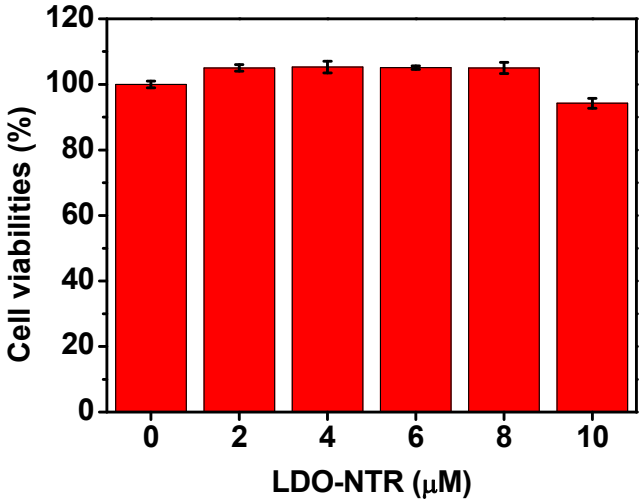

Figure S23. Cell viabilities (%) estimated by MTT proliferation tests versus incubation concentrations of probe. HepG2 cells were incubated with (0, 2, 4, 6, 8, 10 μM) **LDO-NTR** at 37 °C for 24 h.

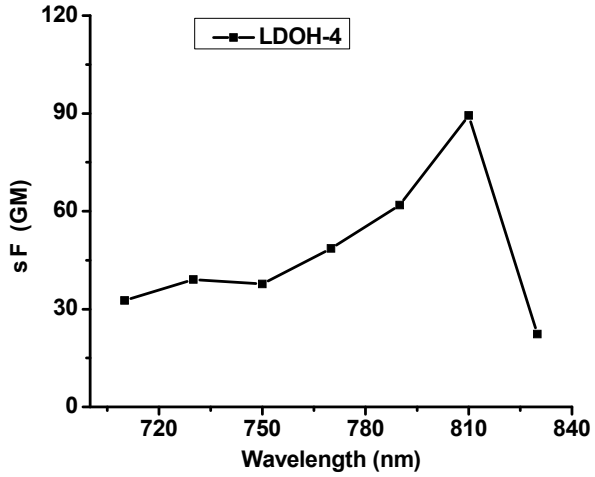

Figure S24. Active TP absorption cross-section of compound **LDOH-4** in PBS containing 20% DMSO.

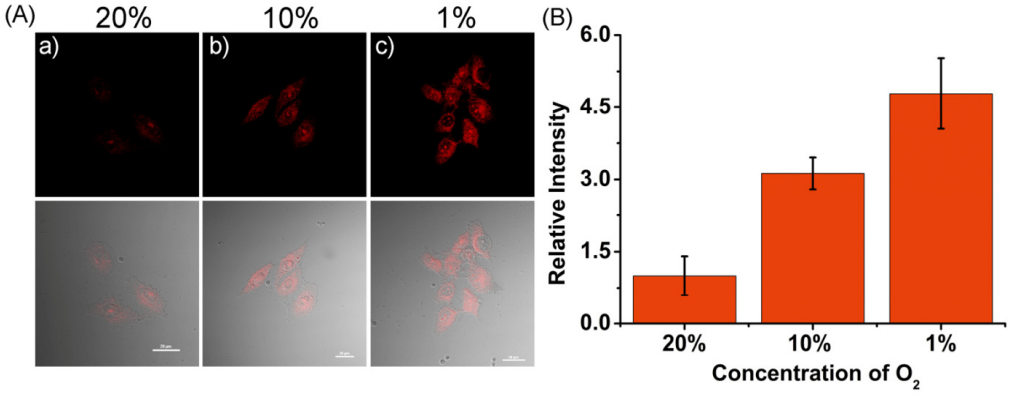

Figure S25. (A) Fluorescence images of HepG2 cells with different pretreatments before incubation with **LDO-NTR** (5 μM, 30 min) by one-photon ($\lambda_{ex}/\lambda_{em}$ = 561/570-620 nm) confocal imaging. From left to right: cells incubated under different oxygen conditions (20%, 10%, and 1%) (a-c) for 5 h, respectively. (B) Relative fluorescence intensity of HepG2 cells in Figure S25A. Scale bar: 20 μm.

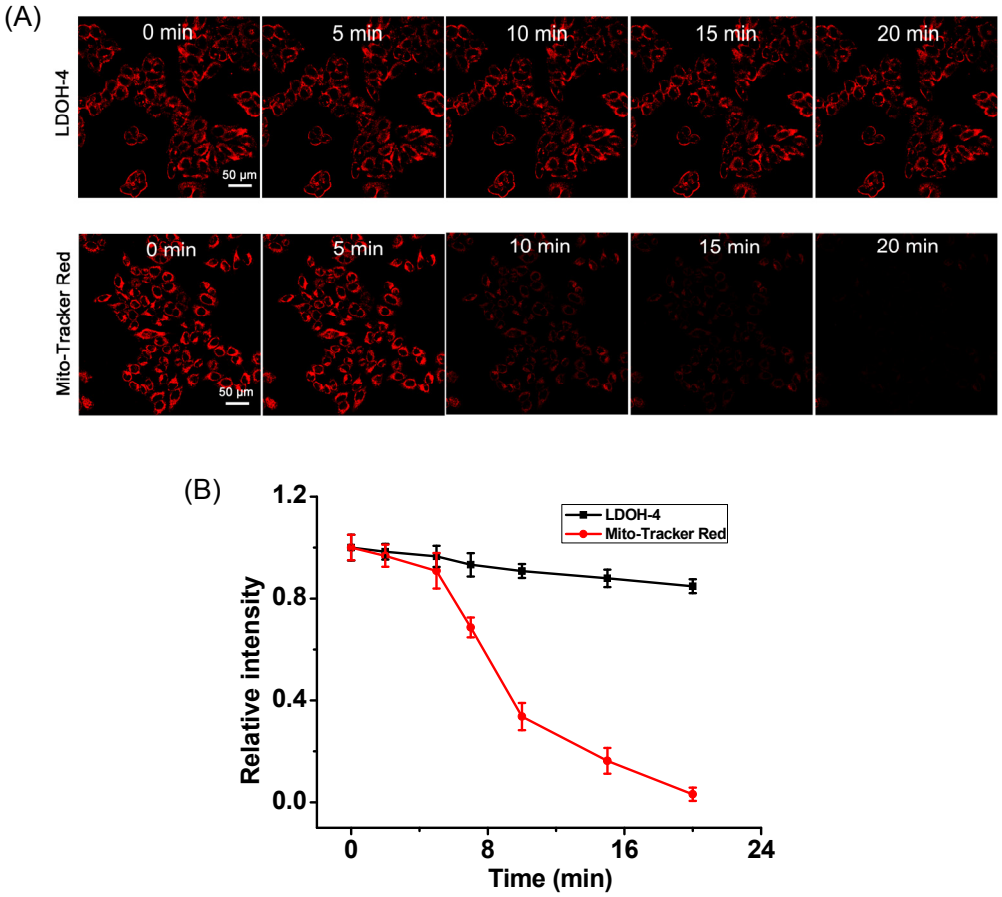

Figure S26. (A) Confocal fluorescence images of living HepG2 cells cultured with **LDOH-4** (1.0 μM) and **Mito-Tracter Red** (1.0 μM) with continuous irradiation using confocal microscope with the same parameters. (B) Quantification of the relative mean fluorescence levels of cells from the images of **LDOH-4** and **Mito-Tracter Red**. Scale bar = 50 μm. λ_{ex} = 561 nm, λ_{em} = 570-620 nm.

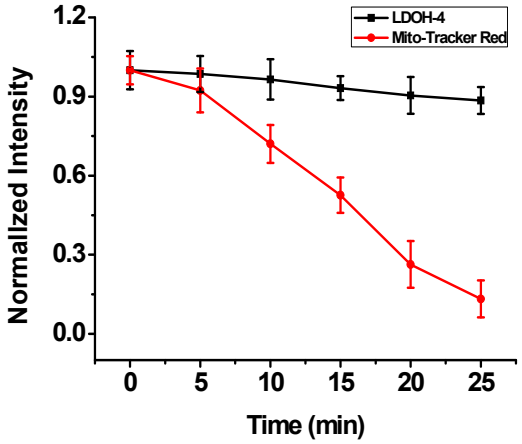

Figure S27. Photostability of **LDOH-4** and **Mito-Tracker Red** in PBS buffer solution (pH 7.4, 25 mM, DMSO:

PBS=2 : 8). The samples were continuously irradiated by white light (50 W) in ice-bath condition.

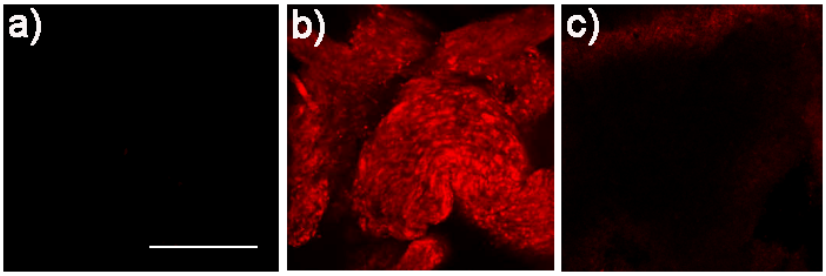

Figure S28. Fluorescence images of tumor tissues by one-photon confocal imaging. a: intact tumor tissues. b: the tumor mice were injected **LDO-NTR** (500 μM, 50 μL) for 1.5 h in situ, then the tumor was sectioned after being anaesthetized. c: the tumor mice were pre-injected with DC (1 mM, 50 μL) for 30 min before with **LDO-NTR** (500 μM, 50 μL) for 1.5 h in situ, then the tumor was sectioned after being anaesthetized. Scale bar = 100 μm. λ_{ex} = 561 nm, λ_{em} = 570-620 nm.

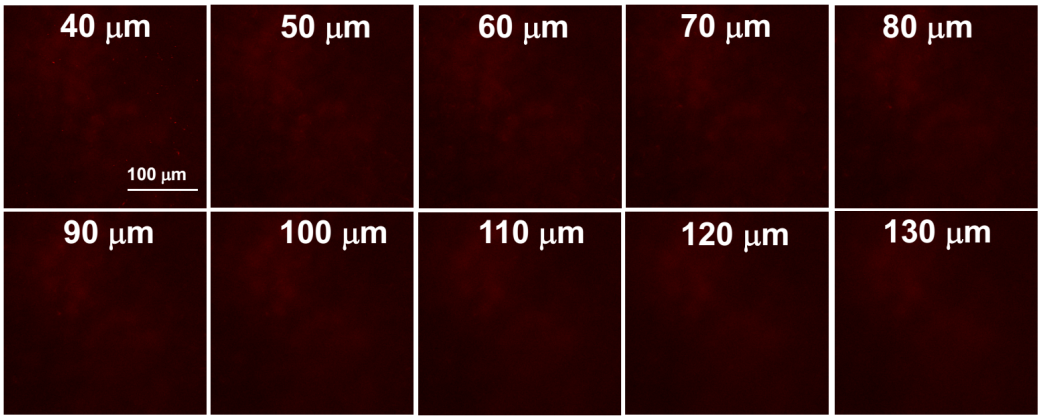

Figure S29. Two-photon fluorescence images of tumor tissues of tumor mice pre-injected with DC (1 mM, 50 μL) for 30 min before with **LDO-NTR** (500 μM, 50 μL) for 1.5 h in situ at the depths of approximately 40~130 μm. Scale bar = 100 μm. λ_{ex} = 561 nm, λ_{em} = 570-620 nm.

10.NMR spectra

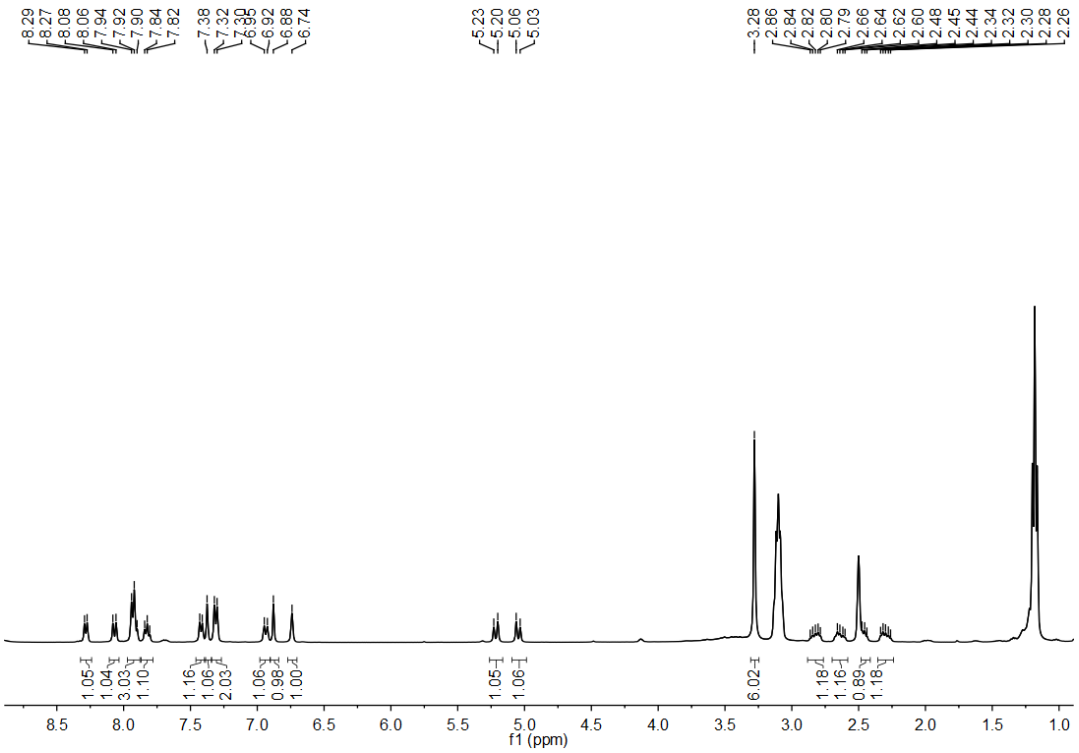

Figure S30. ^{1}H NMR spectra of **LDO-NTR** in DMSO-d_6.

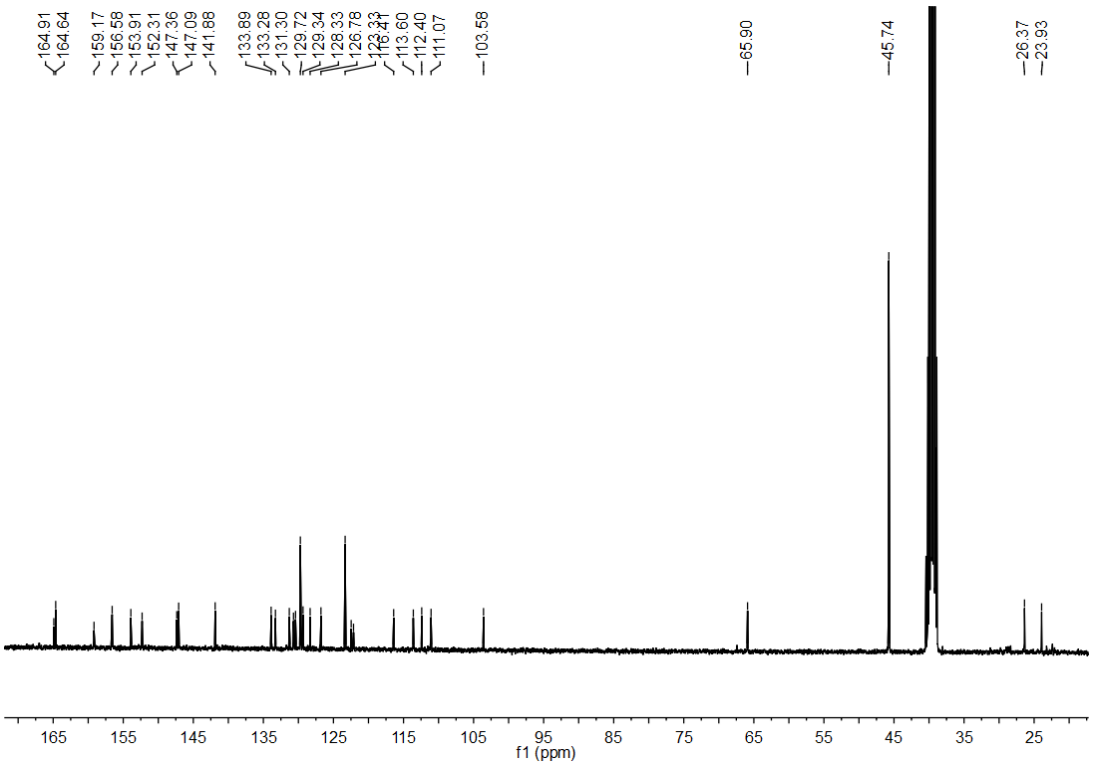

Figure S31. ^{13}C NMR spectrum of **LDO-NTR** in DMSO-d_6.

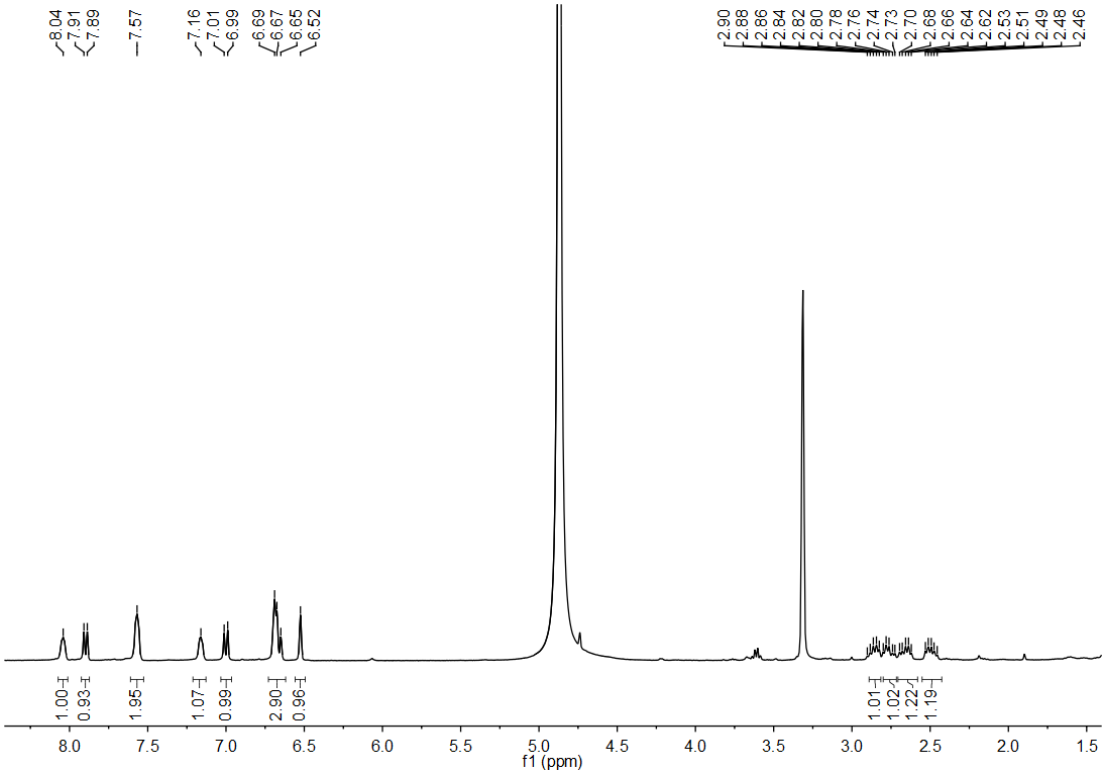

Figure S32. ^{1}H NMR spectra of **LDOH-1** in CD_3OD.

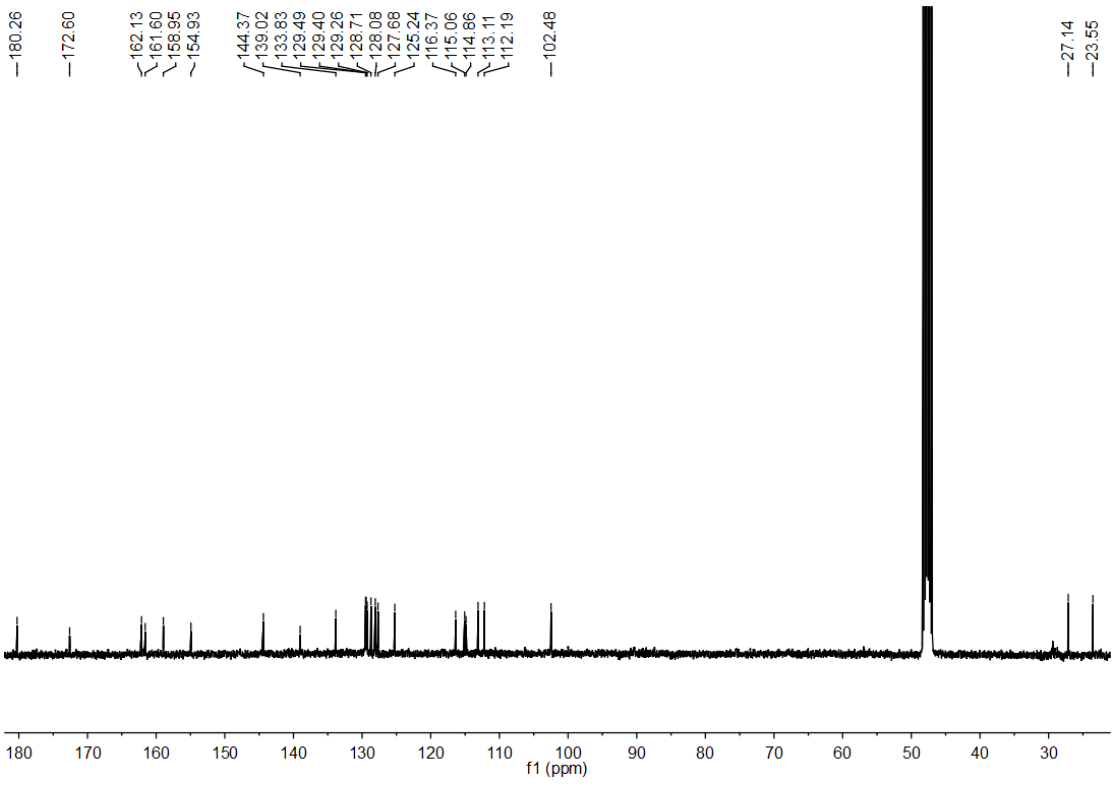

Figure S33. ^{13}C NMR spectrum of **LDOH-1** in CD_3OD

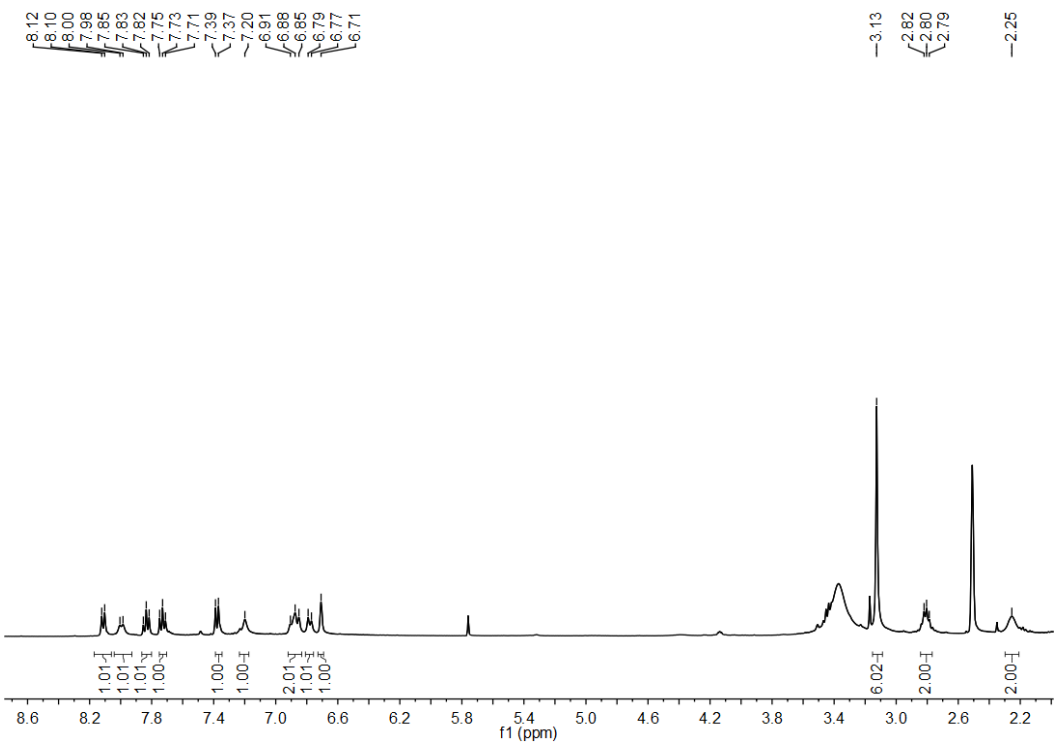

Figure S34. [1]H NMR spectra of **LDOH-2** in DMSO-d_6.

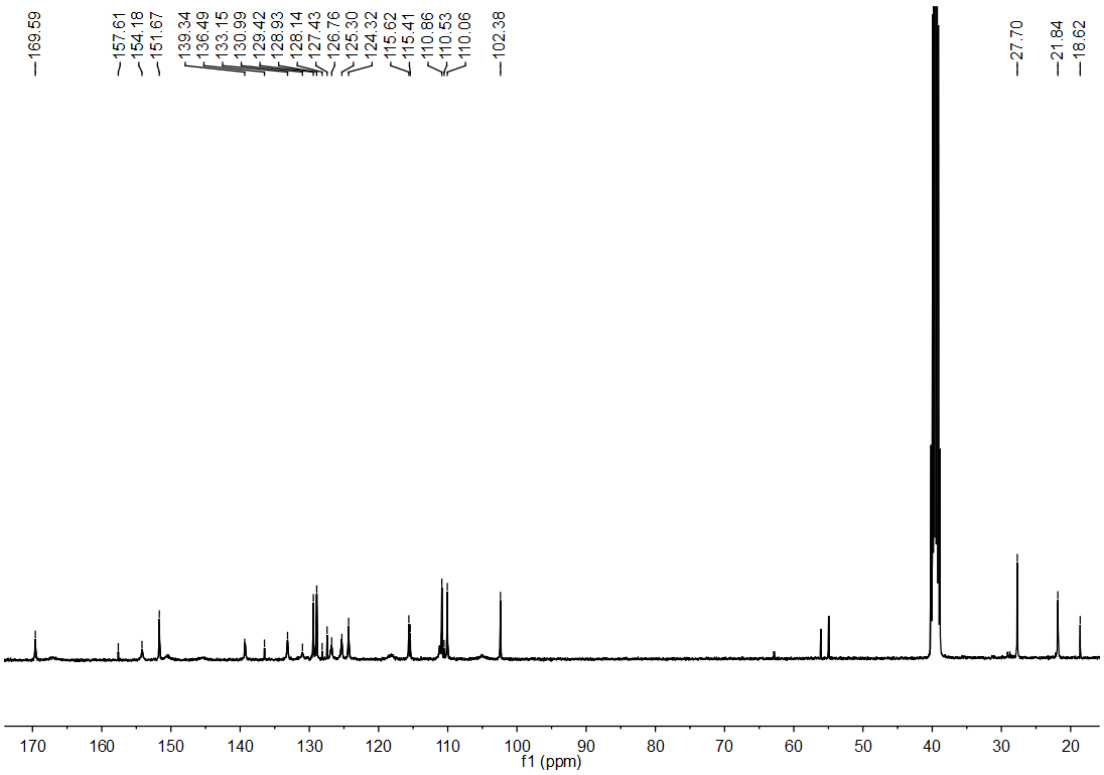

Figure S35. [13]C NMR spectrum of **LDOH-2** in DMSO-d_6.

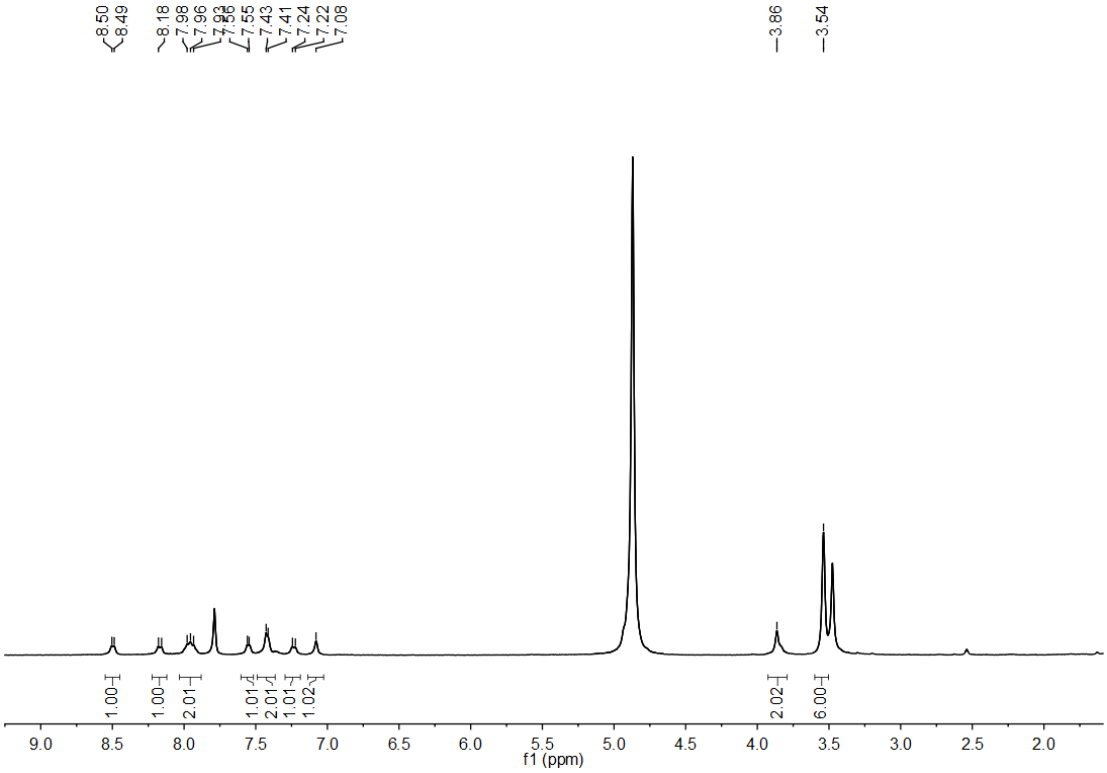

Figure S36. ^{1}H NMR spectra of **LDOH-3** in CD_3OD.

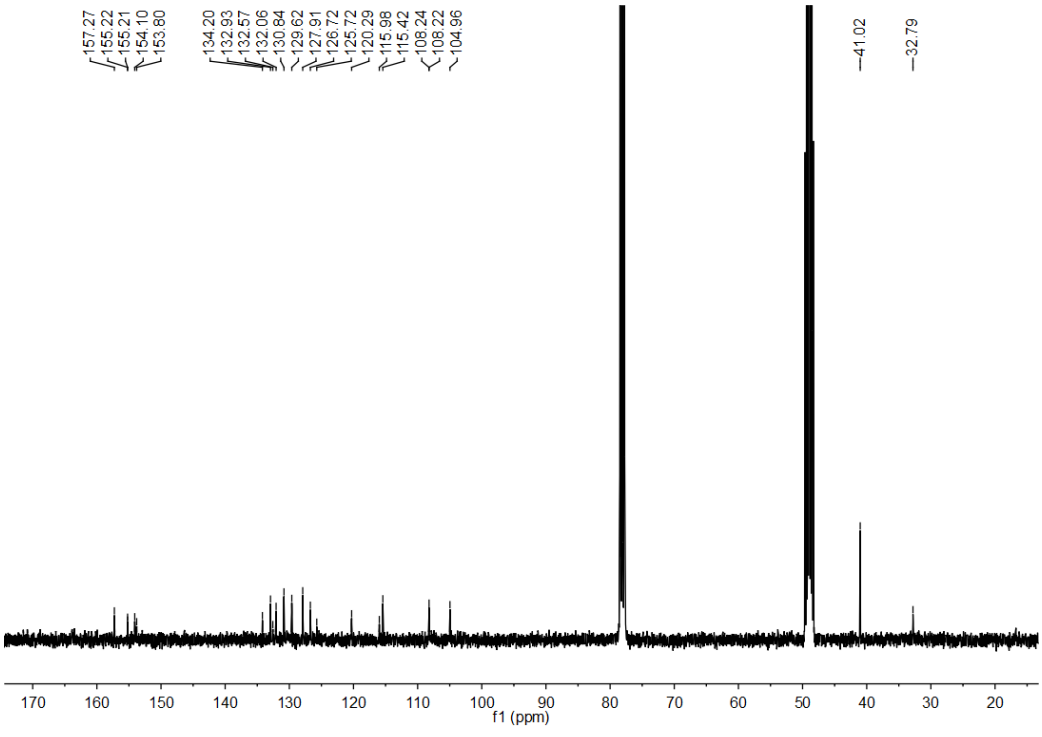

Figure S37. ^{13}C NMR spectrum of **LDOH-3** in CD_3OD+$CDCl_3$.

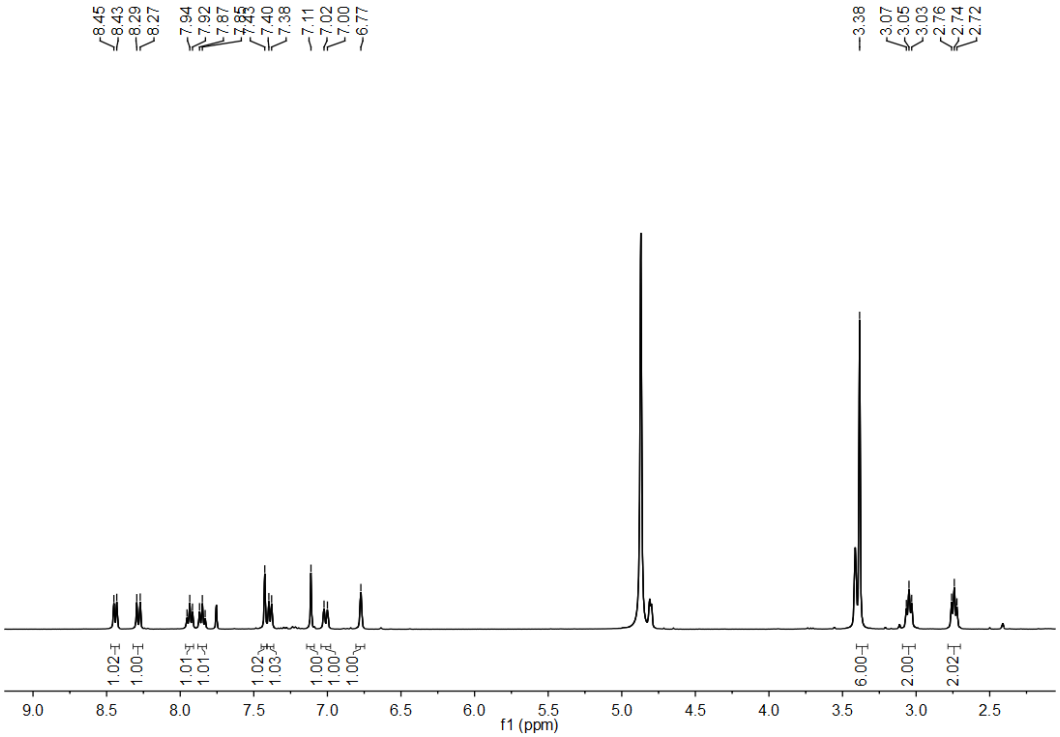

Figure S38. ^{1}H NMR spectra of **LDOH-4** in CD_3OD.

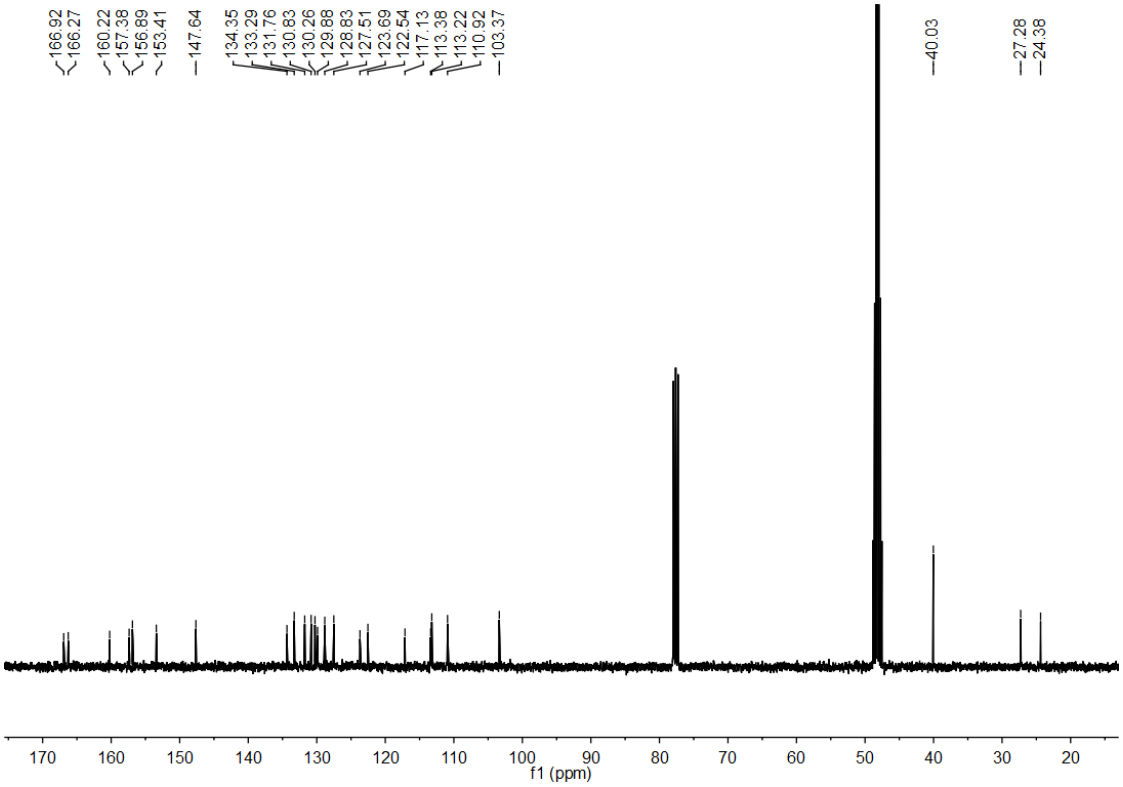

Figure S39. ^{13}C NMR spectrum of **LDOH-4** in CD_3OD+$CDCl_3$.

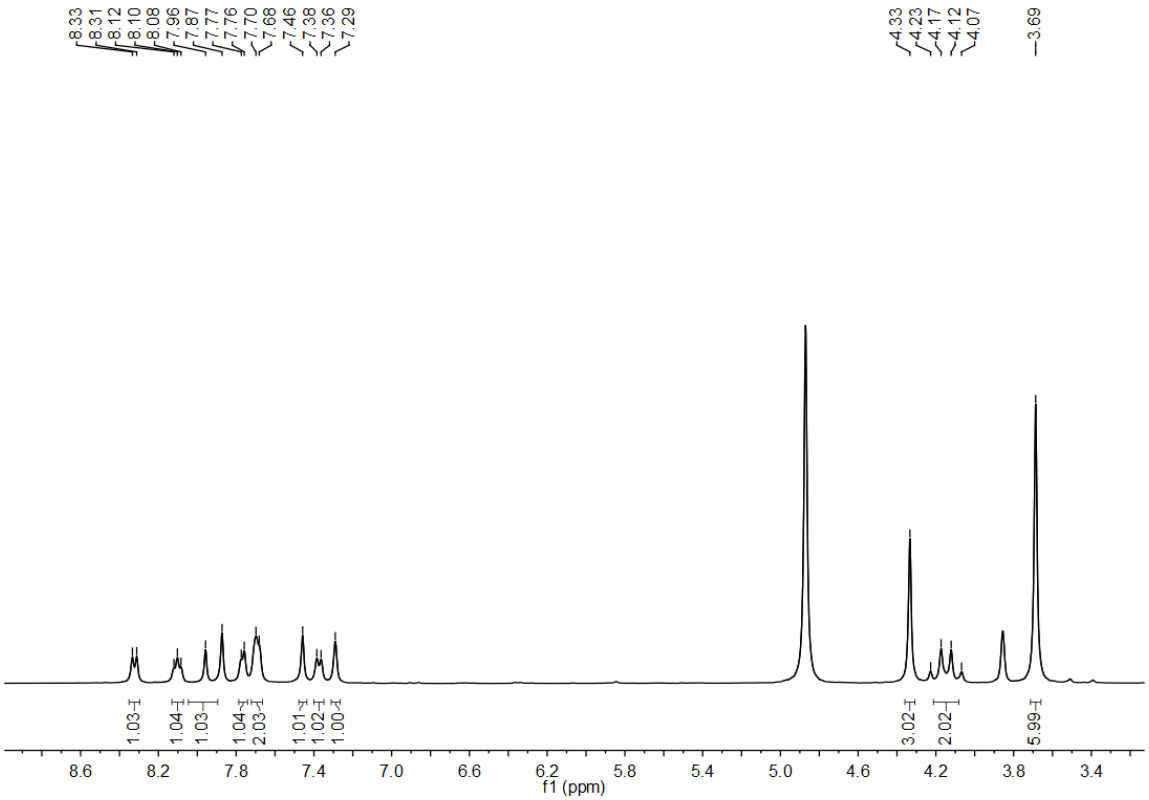

Figure S40. ^{1}H NMR spectra of **Ctrl-1** in CD_3OD.

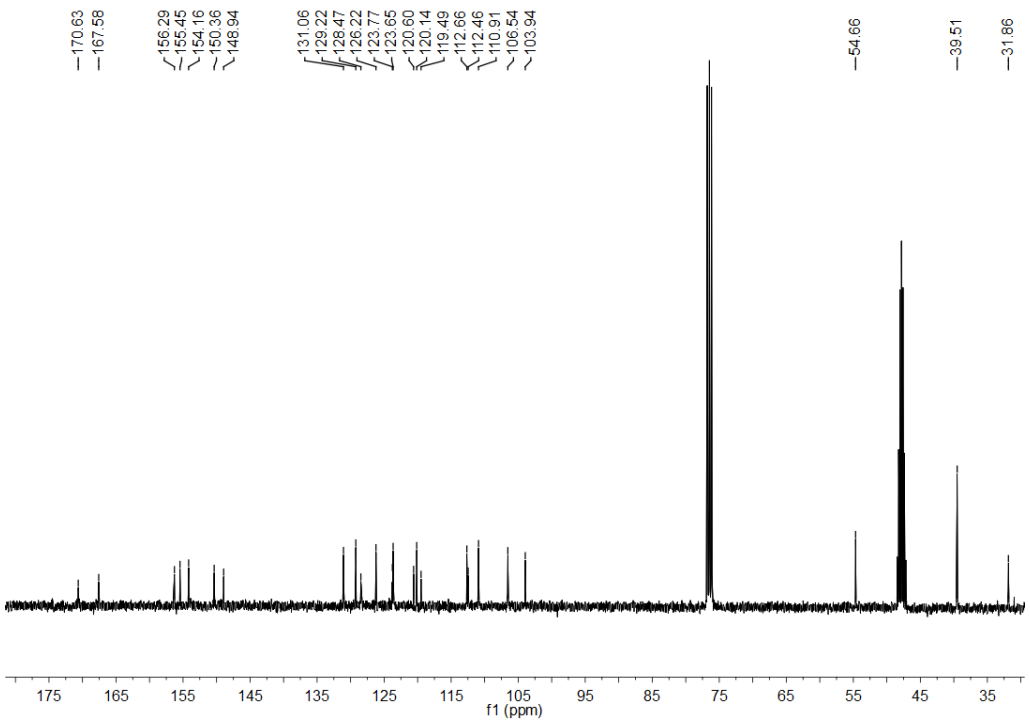

Figure S41. ^{13}C NMR spectrum of **Ctrl-1** in CD_3OD+$CDCl_3$.

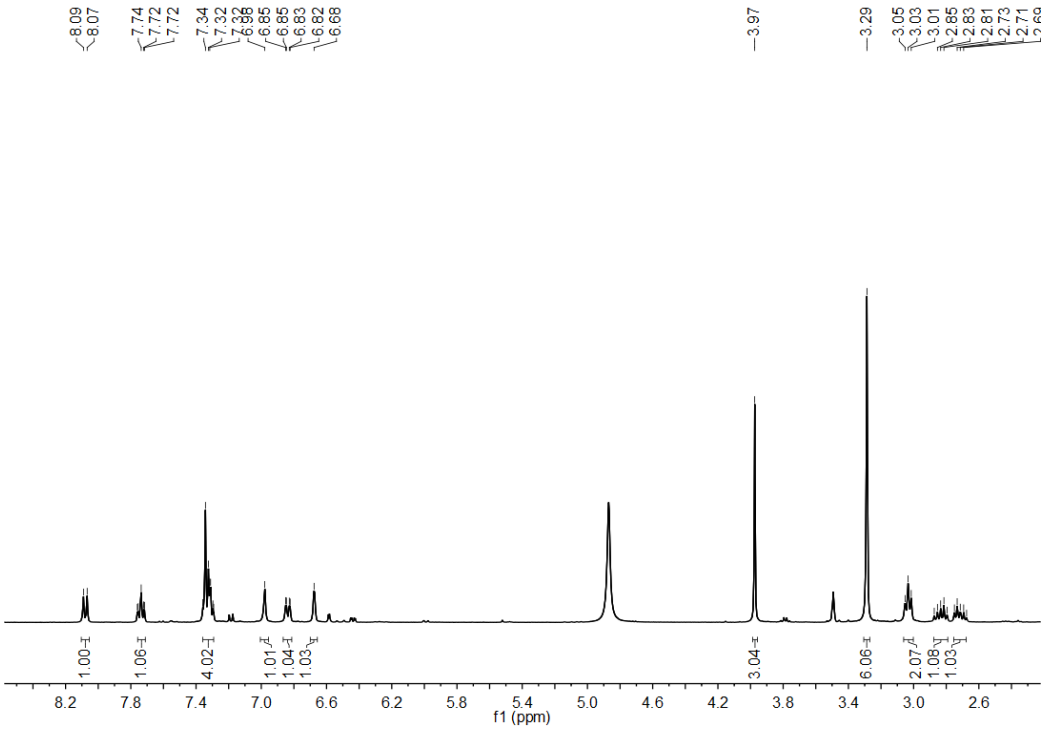

Figure S42. ^{1}H NMR spectra of **Ctrl-2** in CD_3OD.

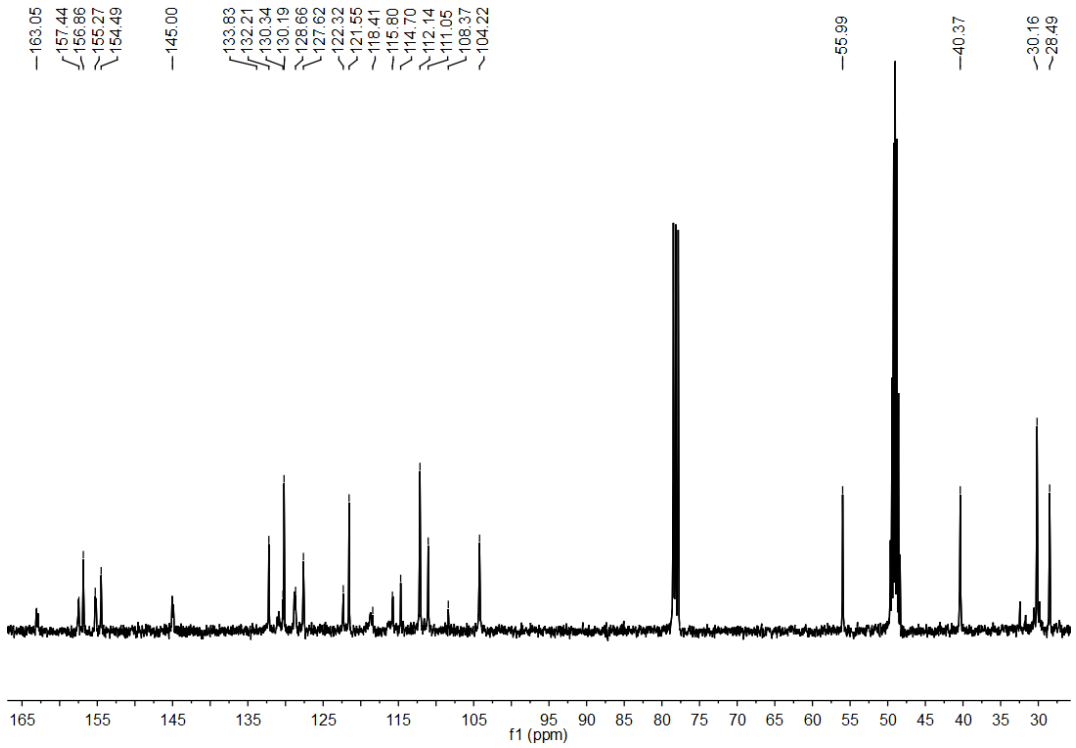

Figure S43. ^{13}C NMR spectrum of **Ctrl-2** in CD_3OD+$CDCl_3$.

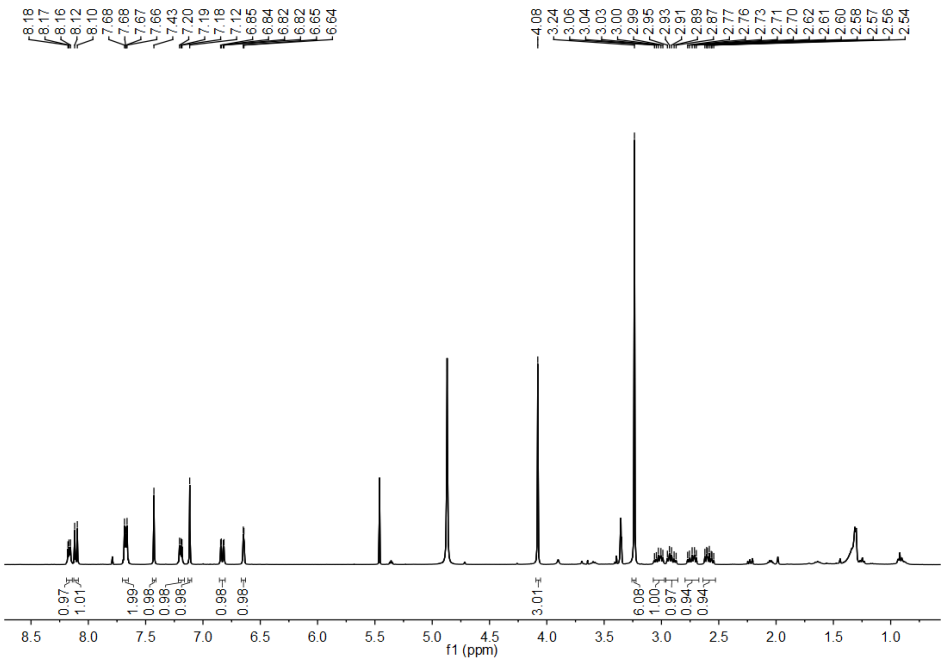

Figure S44. ^{1}H NMR spectrum of **LDO-CH$_3$** in CD_3OD.

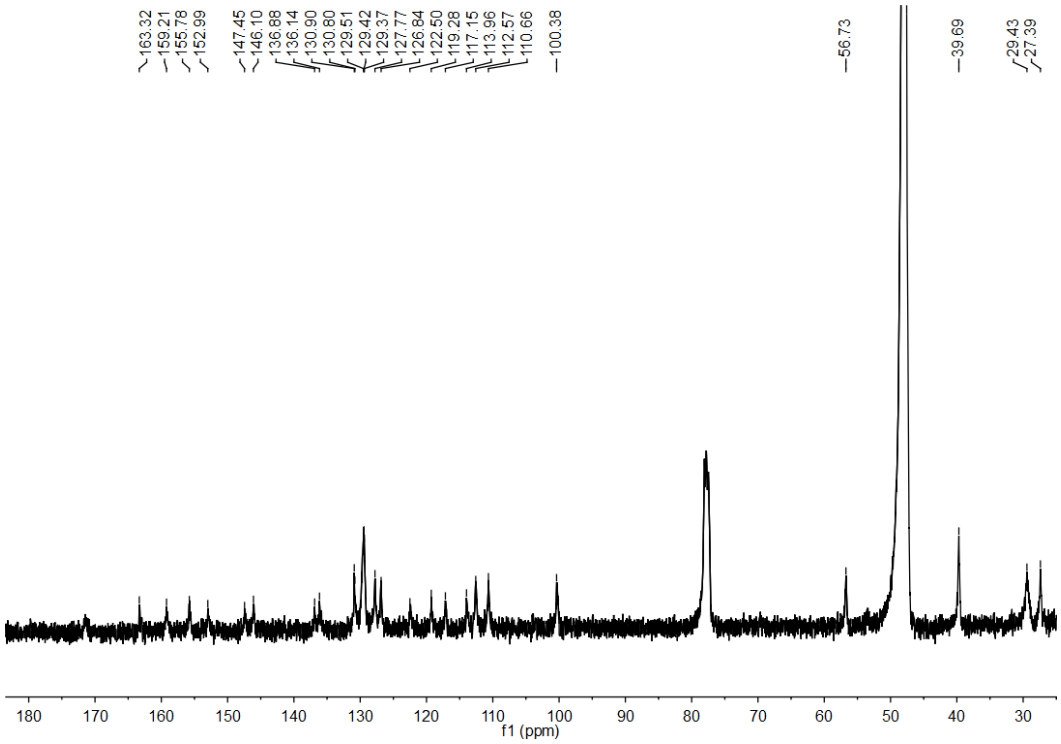

Figure S45. ^{13}C NMR spectrum of **LDO-CH$_3$** in CD_3OD+$CDCl_3$.

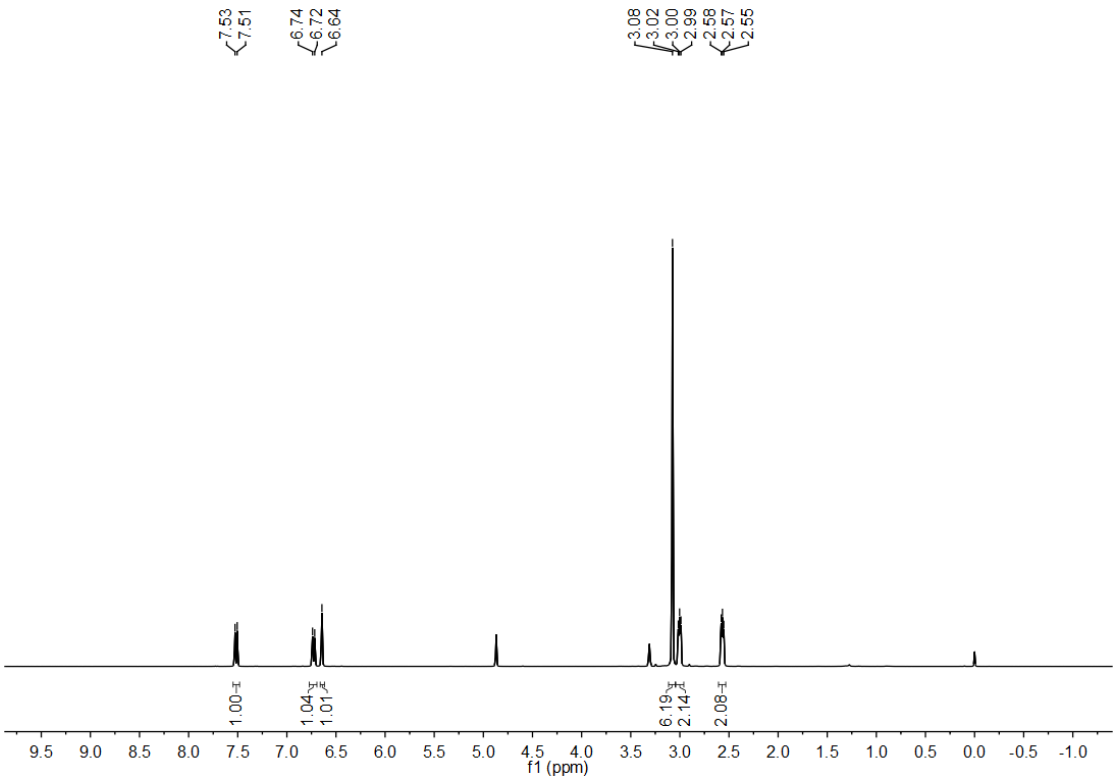

Figure S46. ^{1}H NMR spectra of compound **5** in CD_3OD.

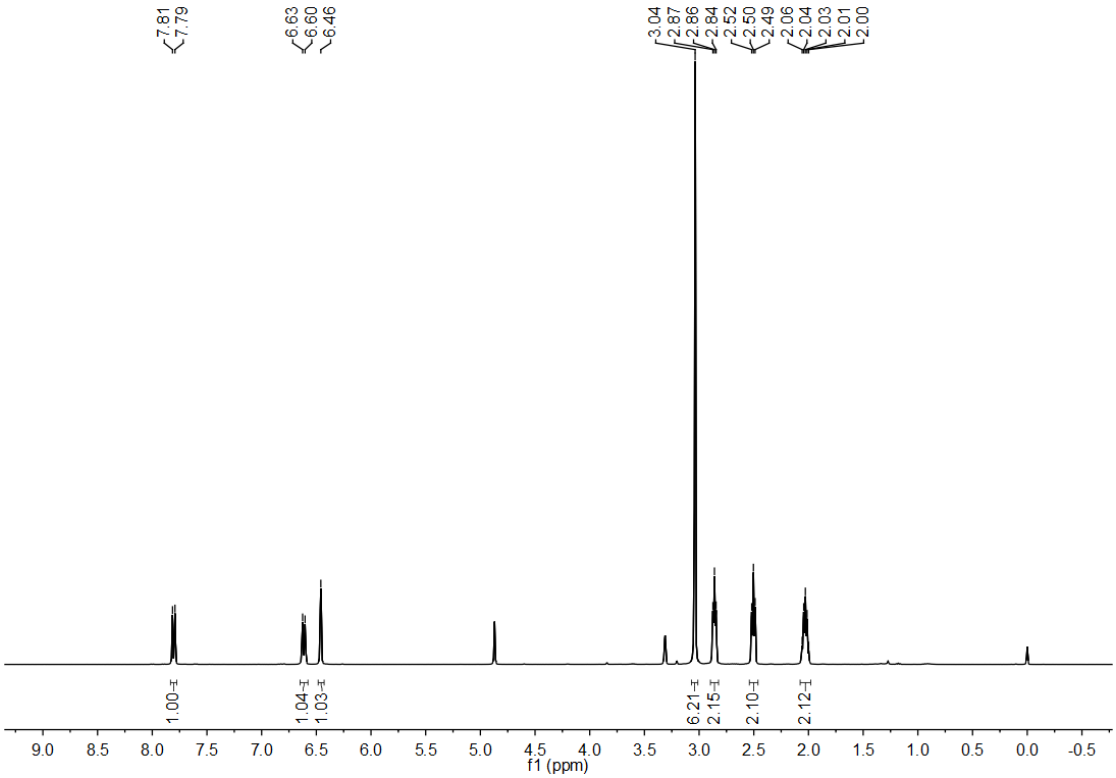

Figure S47. ^{1}H NMR spectra of compound **6** in CD_3OD.

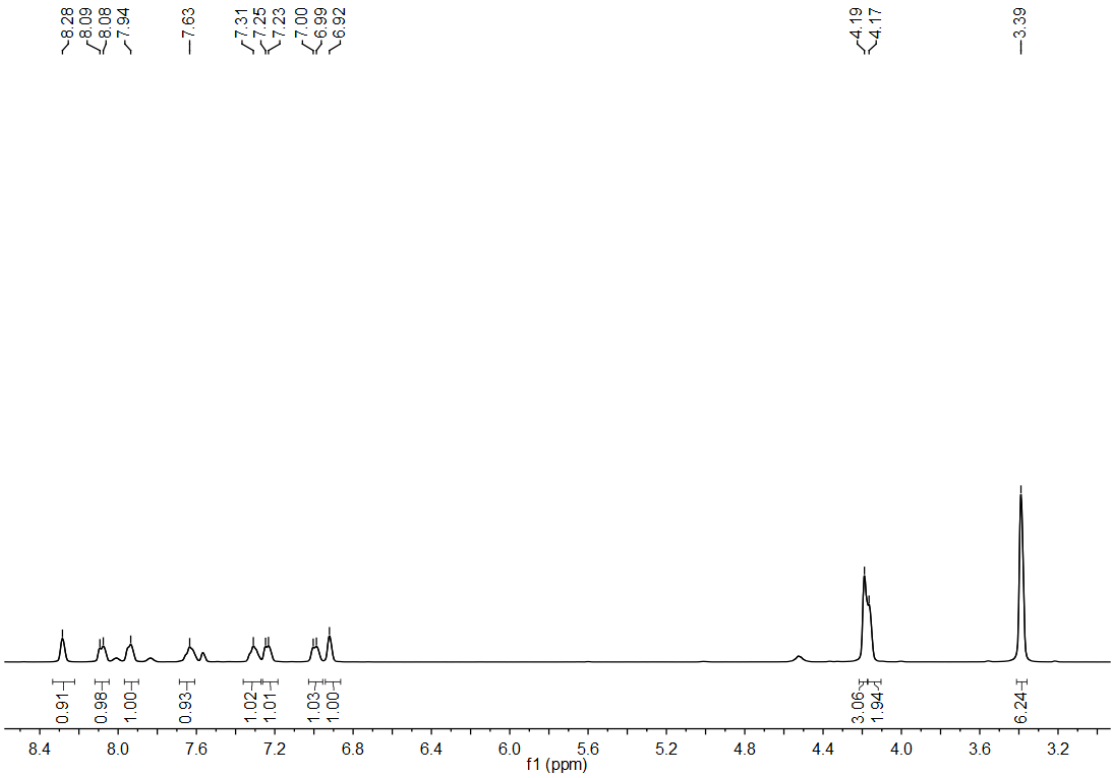

Figure S48. ^{1}H NMR spectra of compound **7** in $CDCl_3$.

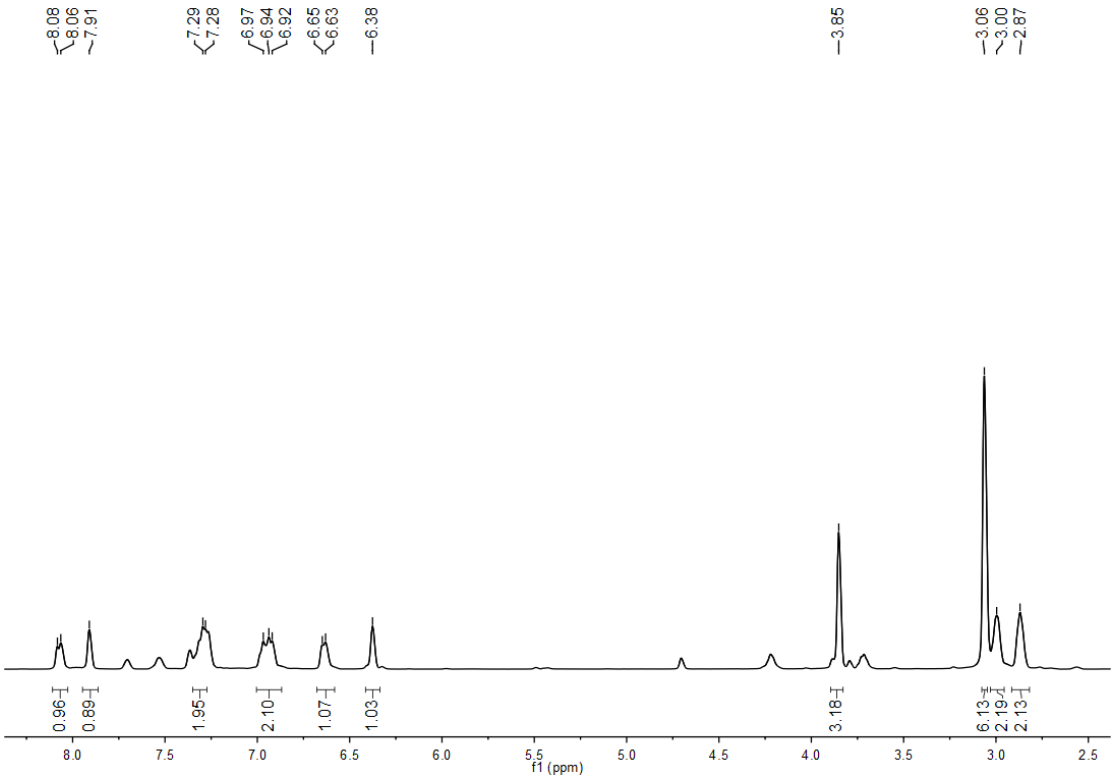

Figure S49. ^{1}H NMR spectra of compound **8** in $CDCl_3$.

11. References

1 Mylon, E.; Roston, S. Effect of tyrosinase upon the fluorimetric determination of epinephrine and arterenol. *Am. J. Physiol*. 1953, **172**, 612-616.

2 Magde, D.; Brannon, J. H.; Cremers, T. L.; Olmsted, J. Absolute Luminescence Yield of Cresyl Violet. A Standard for the Red. *J. Phys. Chem.* 1979, **83**, 696-699.

3 Makarov, N. S.; Drobizhev, M.; Rebane, A. Two-photon absorption standards in the 550-1600 nm excitation wavelength range. *Opt. Express* 2008, **16**, 4029-4047.

4 Xiong, X.; Song, F.; Chen, G.; Sun, W.; Wang, J.; Gao, P.; Zhang, Y.; Qiao, B.; Li, W.; Sun, S.; Fan, J.; Peng, X. Construction of Long-Wavelength Fluorescein Analogues and Their Application as Fluorescent Probes. *Chem. Eur. J.* 2013, **19**, 6538-6545.

5 Wu, D.; Ryu, J.-C.; Chung, Y. W.; Lee, D.; Ryu, J.-H.; Yoon, J.-H.; Yoon, J. A Far-Red-Emitting Fluorescence Probe for Sensitive and Selective Detection of Peroxynitrite in Live Cells and Tissues. *Anal. Chem.* 2017, **89**, 10924-10931.

6 Nicolaou, K. C.; Nilewski, C.; Hale, C. R. H.; Ioannidou, H. A.; ElMarrouni, A.; Koch, L. G. Total Synthesis and Structural Revision of Viridicatumtoxin B. *Angew. Chem. Int. Ed.* 2013, **52**, 8736-8741.

7 Zhang, J.; Liu, H.-W.; Hu, X.-X.; Li, J.; Liang, L.-H.; Zhang, X.-B.; Tan, W. Efficient Two-Photon Fluorescent Probe for Nitroreductase Detection and Hypoxia Imaging in Tumor Cells and Tissues. *Anal. Chem.* 2015, **87**, 11832-11839.

8 Xu, J.; Sun, S.; Li, Q.; Yue, Y.; Li, Y.; Shao, S. A rapid response "Turn-On" fluorescent probe for nitroreductase detection and its application in hypoxic tumor cell imaging. *Analyst* 2015, **140**, 574-581.

9 Li, Y.; Sun, Y.; Li, J.; Su, Q.; Yuan, W.; Dai, Y.; Han, C.; Wang, Q.; Feng, W.; Li, F. Ultrasensitive Near-Infrared Fluorescence-Enhanced Probe for in Vivo Nitroreductase Imaging. *J. Am. Chem. Soc.* 2015, **137**, 6407-6416.

10 Zhai, B.; Hu, W.; Sun, J.; Chi, S.; Lei, Y.; Zhang, F.; Zhong, C.; Liu, Z. A two-photon fluorescent probe for nitroreductase imaging in living cells, tissues and zebrafish under hypoxia conditions. *Analyst* 2017, **142**, 1545-1553.

11 Zhang, X.; Zhao, Q.; Li, Y.; Duan, X.; Tang, Y. Multifunctional Probe Based on Cationic Conjugated Polymers for Nitroreductase-Related Analysis: Sensing, Hypoxia Diagnosis, and Imaging. *Anal. Chem.* 2017, **89**, 5503-5510.

12 Zhu, K.; Qin, T.; Zhao, C.; Luo, Z.; Huang, Y.; Liu, B.; Wang, L. A novel fluorescent turn-on probe for highly selective detection of nitroreductase in tumor cells. *Sensors & Actuators: B. Chemical* 2018, **276**, 397-403.

13 Yang, L.; Niu, J.-Y.; Sun, R.; Xu, Y.-J.; Ge, J.-F. The application of mitochondrial targetable pyronine-pyridinium skeleton in the detection of nitroreductase. *Sensors and Actuators B* 2018, **259**, 299-306.

14 Ao, X.; Bright, S. A.; Taylor, N. C.; Elmes, R. B. P. 2-Nitroimidazole based fluorescent probes for nitroreductase; monitoring reductive stress in cellulo. *Org. Biomol. Chem.* 2017, **15**, 6104-6108.

15 Zhou, Y.; Bobba, K. N.; Lv, X. W.; Yang, D.; Velusamy, N.; Zhang, J. F.; Bhuniy, S. A biotinylated piperazine-rhodol derivative: a 'turn-on' probe for nitroreductase triggered

hypoxia imaging. *Analyst* 2017, **142**, 345-350.

16 Xu, S.; Wang, Q.; Zhang, Q.; Zhang, L.; Zuo, L.; Jiang, J.-D.; Hu, H.-Y. Real time detection of ESKAPE pathogens by a nitroreductase-triggered fluorescence turn-on probe. *Chem. Commun.* 2017, **53**, 11177-11180.

17 Yang, D.; Tian, H. Y.; Zang, T. N.; Li, M.; Zhou, Y.; Zhang, J. F. Hypoxia imaging in cells and tumor tissues using a highly selective fluorescent nitroreductase probe. *Sci. Rep.* 2017, **7**, 9174.

18 Luo, S.; Zou, R.; Wu, J.; Landry, M. P. A Probe for the Detection of Hypoxic Cancer Cells. *ACS Sens.* 2017, **2**, 1139-1145.

19 Zhou, J.; Shi, W.; Li, L.-H.; Gong, Q.-Y.; Wu, X.-F.; Li, X.-H.; Ma, H.-M. A Lysosome-Targeting Fluorescence Off-On Probe for Imaging of Nitroreductase and Hypoxia in Live Cells. *Chem. Asian J.* 2016, **11**, 2719-2724.

20 Xu, A.; Tang, Y.; Ma, Y.; Xu, G.; Gao, S.; Zhao, Y.; Lin, W. A fast-responsive two-photon fluorescent turn-on probe for nitroreductase and its bioimaging application in living tissues. *Sensors and Actuators B* 2017, **252**, 927-933.

21 Guo, T.; Cui, L.; Shen, J.; Zhu, W.; Xu, Y.; Qian, X. A highly sensitive long-wavelength fluorescence probe for nitroreductase and hypoxia: selective detection and quantification. *Chem. Commun.* 2013, **49**, 10820-10822.

22 Li, Z.; He, X.; Wang, Z.; Yang, R.; Shi, W.; Ma, H. In vivo imaging and detection of nitroreductase in zebrafish by a new near-infrared fluorescence off-on probe. *Biosensors and Bioelectronics,* 2015, **63**, 112-116.

23 Zhu, D.; Xue, L.; Li, G.; Jiang, H. A highly sensitive near-infrared ratiometric fluorescent probe for detecting nitroreductase and cellular imaging. *Sensors and Actuators B*, 2016, **222**, 419-424.

24 Xue C.; Lei Y.; Zhang S.; Sha Y. A cyanine-derived “turn-on” fluorescent probe for imaging nitroreductase in hypoxic tumor cells. *Anal. Methods,* 2015, **7**, 10125-10128.

25 Shi, Y.; Zhang, S.; Zhang, X. A novel near-infrared fluorescent probe for selectively sensing nitroreductase (NTR) in an aqueous medium. *Analyst,* 2013, **138**, 1952-1955.

26 Zhang, N.; Wang, Y.; Leng, S.; Xu, S.; Zhang, L.; Wang, Q.; Zhang, Q.; Hu, H.-Y. An efficient fluorescence sensor for nitroreductase selective imaging based on intramolecular photoinduced electron transfer. *Talanta* 2019, **205**, 120133.